CHAOS 2014

Proceedings

7th Chaotic Modeling and Simulation International Conference

Editor

Christos H. Skiadas

7 – 10 June 2014

Lisbon Portugal

Imprint
Proceedings of the 7th Chaotic Modeling and Simulation International Conference (Lisbon, Portugal: 7-10 June, 2014)
Published by: ISAST: International Society for the Advancement of Science and Technology.
Editor: Christos H Skiadas

Preface

7th Chaotic Modeling and Simulation International Conference

7 – 10 June 2014, Lisbon Portugal

It is our pleasure to present the Proceedings of the 7th International Conference (CHAOS2014) on Chaotic Modeling, Simulation and Applications. We support the study of nonlinear systems and dynamics in an interdisciplinary research field and very interesting applications were presented. A forum to exchange ideas, methods, and techniques in the field of Nonlinear Dynamics, Chaos, Fractals and their applications in General Science and in Engineering Sciences was established.

The principal aim of CHAOS2014 International Conference was to expand the development of the theories of the applied nonlinear field, the methods and the empirical data and computer techniques, and the best theoretical achievements of chaotic theory as well.

Chaotic Modeling and Simulation Conferences continue to grow considerably from year to year thus making a well established platform to present and disseminate new scientific findings and interesting applications. We thank all the contributors to the success of this conference and especially the authors of this *Conference Proceedings* of CHAOS 2014.

Special thanks to the Scientific Committee, the ISAST Committee, the Conference Secretary Mary Karadima and all the members of the Secretariat.

September 2014
Christos H. Skiadas
Conference Chair

Honorary Committee

Leon O. Chua
EECS Department, University of California, Berkeley, USA
Editor of the International Journal of Bifurcation and Chaos

Gennady A. Leonov
Dean of Mathematics and Mechanics Faculty, Saint-Petersburg State University, Russia
Member (corresponding) of Russian Academy of Science

David Ruelle
Academie des Sciences de Paris
Honorary Professor at the Institut des Hautes Etudes Scientifiques of Bures-sur-Yvette, France

Ferdinand Verhulst
Mathematics Faculty, Utrecht, The Netherlands

International Scientific Committee

C. H. Skiadas (Technical University of Crete, Chania, Greece), Chair
H. Adeli (The Ohio State University, USA)
J.-O. Aidanpaa (Division of Solid Mechanics, Lulea University of Technology, Sweden)
N. Akhmediev (Australian National University, Australia)
M. Amabili (McGill University, Montreal, Canada)
J. Awrejcewicz (Technical University of Lodz, Poland)
E. Babatsouli (University of Crete, Rethymnon, Greece)
J. M Balthazar (UNESP-Rio Claro, State University of Sao Paulo, Brasil)
S. Bishop (University College London, UK)
T. Bountis (University of Patras, Greece)
Y. S. Boutalis (Democritus University of Thrace, Greece)
C. Chandre (Centre de Physique Theorique, Marseille, France)
M. Christodoulou (Technical University of Crete, Chania, Crete, Greece)
P. Commendatore (Universita di Napoli 'Federico II', Italy)
D. Dhar (Tata Institute of Fundamental Research, India)
J. Dimotikalis (Technological Educational Institute, Crete, Greece)
B. Epureanu (University of Michigan, Ann Arbor, MI, USA)
G. Fagiolo (Sant'Anna School of Advanced Studies, Pisa, Italy)
M. I. Gomes (Lisbon University and CEAUL, Lisboa, Portugal)
V. Grigoras (University of Iasi, Romania)
A. S. Hacinliyan (Yeditepe University, Istanbul, Turkey)
K. Hagan, (University of Limerick, Ireland)

Plenary and Keynote Talks

Walter Gekelman
University of California, Los Angeles, CA, USA

Entropy, Complexity and Chaos in Magnetic Flux Ropes

Alexander G Ramm
Department of Mathematics, Kansas State University, USA

Wave scattering by many small particles and creating materials with desired refraction coefficients

Leszek Sirko
Institute of Physics, Polish Academy of Sciences, Warszawa, Poland

The Resonances and Poles in Isoscattering Microwave Networks and Graphs

Lev S. Tsimring
BioCircuits Institute, University of California - San Diego, La Jolla, CA, USA

Generation and Synchronization of Oscillations in Synthetic Gene Networks

Contents

Governance of Alteration of the Deformation Field States of Fractal Volumetric Structures in a Multilayer Nanosystem

Olga P. Abramova, Sergey V. Abramov

Donetsk National University, Ukraine
E-mail: oabramova@ua.fm

Abstract: For a multilayer nanosystem various types of fractal volumetric structures are obtained. The singular points (attractors) of the deformation field of these structures are located on fractal quasi-two-dimensional surfaces. This uses the theory of fractional calculus and the concept of fractal. The influence of translation and rotation on the deformation field states of these structures is shown. The interaction of nodes both in the plane of the basic rectangular discrete lattice and the interplanar interactions is taken into account. Using spatial rotation (external governance) the alteration of the states of fractal volumetric structures can be carried out. This allows also to fulfill a stochastic (due to changes in the internal parameters, the process of self-organization) governing of the alteration of these structures. The analysis in terms of averaged functions makes it possible to identify the features of the behavior and conditions of the transition from one structure to another.
Keywords: fractal volumetric structures, stochastic deformation field, averaged functions, alteration of the structure, multilayer nanosystem.

1. Introduction

Investigating the fundamental properties of multilayer nanosystems and nanomaterials [1 - 4] is actual for the modern areas of nanotechnology, structural and non-linear mechanics [5]. The active nanostructural elements in real and artificial nanosystems are clusters, pores, quantum dots, wells, two-dimensional quantum billiards (quantum corrals) [6]. These elements can find their application in quantum information science, nanomechanics, quantum optics, and for the quantum computers, molecular spin memory devices [3]. The theoretical description of the chaotic states in the structural mechanics, analysis of nonlinear dynamical models of attractors and the chaotic simulation are discussed in the books [5 - 8].

Fractal dislocation [9 - 12] is one of the non-classical active nanostructural objects in a model nanosystem. In paper [10] the possibility of an appearance of quasi-two-dimensional structures of fractal elliptic and hyperbolic dislocations, fractal quantum dot was investigated. The analysis of the behavior of the averaged functions allows to determine the critical values of the governing parameters. In papers [11 - 13] a possibility of governing the alteration of the deformation field of fractal quasi-two-dimensional structures in model nanosystems was shown. In this case accounting the interplanar interactions in multilayer nanosystem can lead to the formation of fractal volumetric structures. The possibility of constructing fractal nanotraps based on quasi-two-dimensional fractal structures and governing the behavior of coupled systems:

7th CHAOS Conference Proceedings, 7-10 June 2014, Lisbon Portugal
C. H. Skiadas (Ed)

fractal trap – fractal structure were discussed in [12].
The purpose of this paper is to describe the features of the behavior of deformation fields of fractal volumetric structures, the study of the possibilities of external and internal governance of structure alteration in the multilayer model nanosystem.

2. Classification of fractal volumetric structures

We consider a model nanosystem [10, 11]: volumetric discrete lattice $N_1 \times N_2 \times N_3$, whose nodes are given by integers n, m, j ($n = \overline{1, N_1}$; $m = \overline{1, N_2}$; $j = \overline{1, N_3}$). Dimensionless variable displacement u of lattice node is described by analogy with [10], but with a changed value Q

$$u = (1-\alpha)(1-2\,\mathrm{sn}^2(u-u_0,k))/Q\,. \qquad (1)$$

Here α is the fractal dimension of the deformation field u along the Oz-axis ($\alpha \in [0,1]$); u_0 is the constant (critical) displacement; k is the modulus of the elliptic sine. The changed value Q considers both the interaction of the nodes in the main plane of rectangular discrete lattice and the interplanar interactions. This allows to fulfill a stochastic (due to changes in the internal parameters, the process of self-organization) governing of the alteration of emerging structures. The initial expression for Q has the form

$$Q = p_0' + p_1' n + p_2' m + p_3' j - b_1\left(\frac{n'-n_0}{n_c}\right)^2 - b_2\left(\frac{m'-m_0}{m_c}\right)^2 - b_3\left(\frac{j'-j_0}{j_c}\right)^2. \qquad (2)$$

The expression (2) has thirteen parameters. The parameter p_0' is independent of the variables n, m, j; parameters p_1', p_2', p_3' are included in the linear form; parameters b_1, b_2, b_3, n_0, n_c, m_0, m_c, j_0, j_c determine the behavior of the quadratic form. Parameters n_c, m_c, j_c play the role of semi-axes of fractal volumetric structures in a new coordinate system $O'n'm'j'$. The original coordinate system $Onmj$ is described in terms of variables n, m, j.
Perform spatial axis rotation of the coordinate system around axis Oj, move from the system $Onmj$ to the system $O'n'm'j'$ by the formulas

$$n' = n \cdot k_1' \,\mathrm{cn}(u_{1\beta}, k_1) - m \cdot \mathrm{sn}(u_{1\beta}, k_1) + j \cdot k_1 \,\mathrm{cn}(u_{1\beta}, k_1);$$

$$m' = n \cdot k_1' \,\mathrm{sn}(u_{1\beta}, k_1) + m \cdot \mathrm{cn}(u_{1\beta}, k_1) + j \cdot k_1 \,\mathrm{sn}(u_{1\beta}, k_1);$$

$$j' = -n \cdot k_1 + j \cdot k_1';\ k_1 = \mathrm{sn}(u_{1\theta}, k_{1\theta});\ k_1' = \mathrm{cn}(u_{1\theta}, k_{1\theta});\ k_1^2 + k_1'^2 = 1. \qquad (3)$$

Here the dimensionless displacement $u_{1\beta}$ is connected with the polar angle $\varphi_{1\beta}$ in the plane Onm by relation $u_{1\beta} = F(\varphi_{1\beta}, k_1)$; F is an incomplete elliptic integral of the first kind; the dimensionless displacement $u_{1\theta}$ is connected with the effective angle θ_1 by relation $u_{1\theta} = F(\theta_1, k_{1\theta})$; $k_1, k_{1\theta}$ are modules of elliptic functions. The dimensionless displacement $u_{1\beta}$ is a nonlinear function of the two parameters $\varphi_{1\beta}$ and k_1, that define the different mechanisms of alteration of fractal volumetric structure and governing it. Here the parameter k_1 is a nonlinear function of $u_{1\theta}$ and $k_{1\theta}$. As a result, the displacement $u_{1\beta}$ becomes a complex function depending on three parameters $\varphi_{1\beta}$, $u_{1\theta}$, $k_{1\theta}$. Note that for $k_{1\theta} = 0$ from (3) we obtain

$$k_1 = \mathrm{sn}(u_{1\theta}, 0) = \sin\theta_1; \quad k_1' = \mathrm{cn}(u_{1\theta}, 0) = \cos\theta_1. \tag{4}$$

For $\theta_1 = n_{\theta 1}\pi$, where $n_{\theta 1} = 0; \pm 1; \pm 2; \ldots$ from expressions (3) by using (4) follow relations

$$k_1 = 0; \quad k_1' = (-1)^{n_{\theta 1}}; \quad \mathrm{sn}(u_{1\beta}, k_1) = \sin\varphi_{1\beta}; \quad \mathrm{cn}(u_{1\beta}, k_1) = \cos\varphi_{1\beta};$$

$$n' = n\cdot(-1)^{n_{\theta 1}}\cos\varphi_{1\beta} - m\cdot\sin\varphi_{1\beta}; \; m' = n\cdot(-1)^{n_{\theta 1}}\sin\varphi_{1\beta} + m\cdot\cos\varphi_{1\beta}; \; j' = j(-1)^{n_{\theta 1}}. \tag{5}$$

Expressions (5) for even values $n_{\theta 1} = 0; \pm 2; \ldots$ earlier used to describe the effect of rotation in the plane Onm on the deformation field state of fractal quasi-two-dimensional structures. In contrast to (5) of the expression (3) take into account the spatial rotation of volumetric structure. For $\theta_1 = (2n_{\theta 1} + 1)\pi / 2$ from expressions (3) by using (4) follow relations

$$k_1 = (-1)^{n_{\theta 1}}; \quad \mathrm{sn}(u_{1\beta}, k_1) = \mathrm{th}(u_{1\beta}); \quad \mathrm{cn}(u_{1\beta}, k_1) = \mathrm{sech}(u_{1\beta}); \quad j' = -n(-1)^{n_{\theta 1}};$$

$$n' = -m\cdot\mathrm{th}(u_{1\beta}) + j\cdot(-1)^{n_{\theta 1}}\,\mathrm{sech}(u_{1\beta}); \; m' = m\cdot\mathrm{sech}(u_{1\beta}) + j\cdot(-1)^{n_{\theta 1}}\,\mathrm{th}(u_{1\beta}). \tag{6}$$

If $k_{1\theta} = 1$, then for k_1, k_1' from (3) we obtain

$$k_1 = \mathrm{sn}(u_{1\theta}, 1) = \mathrm{th}(u_{1\theta}); \quad k_1' = \mathrm{cn}(u_{1\theta}, 1) = \mathrm{sech}(u_{1\theta}). \tag{7}$$

It follows that if $u_{1\theta} = 0$, then $k_1 = 0$, $k_1' = 1$. For $u_{1\theta} \to \pm\infty$ we obtain $k_1 = \pm 1$, $k_1' = 0$, respectively. Finite values $u_{1\theta} = u_{10} \neq 0$ define specific intermediate values $k_1 = \mathrm{th}(u_{10})$, $k_1' = \mathrm{sech}(u_{10})$.

Performing spatial axis rotation of the coordinate system around axis Om, we move from the system $Onmj$ to the system $O'n'm'j'$ by the formulas

$$j' = j \cdot k_2' \operatorname{cn}(u_{2\beta}, k_2) - n \cdot \operatorname{sn}(u_{2\beta}, k_2) + m \cdot k_2 \operatorname{cn}(u_{2\beta}, k_2);$$

$$n' = j \cdot k_2' \operatorname{sn}(u_{2\beta}, k_2) + n \cdot \operatorname{cn}(u_{2\beta}, k_2) + m \cdot k_2 \operatorname{sn}(u_{2\beta}, k_2);$$

$$m' = -j \cdot k_2 + m \cdot k_2';\ k_2 = \operatorname{sn}(u_{2\theta}, k_{2\theta});\ k_2' = \operatorname{cn}(u_{2\theta}, k_{2\theta});\ k_2^2 + k_2'^2 = 1. \quad (8)$$

Here the dimensionless displacement $u_{2\beta}$ is connected with the polar angle $\varphi_{2\beta}$ in the plane Ojn by relation $u_{2\beta} = F(\varphi_{2\beta}, k_2)$; the dimensionless displacement $u_{2\theta}$ is connected with the effective angle θ_2 by relation $u_{2\theta} = F(\theta_2, k_{2\theta})$; $k_2, k_{2\theta}$ are modules of elliptic functions.

Performing spatial axis rotation of the coordinate system around axis On, we move from the system $Onmj$ to the system $O'n'm'j'$ by the formulas

$$m' = m \cdot k_3' \operatorname{cn}(u_{3\beta}, k_3) - j \cdot \operatorname{sn}(u_{3\beta}, k_3) + n \cdot k_3 \operatorname{cn}(u_{3\beta}, k_3);$$

$$j' = m \cdot k_3' \operatorname{sn}(u_{3\beta}, k_3) + j \cdot \operatorname{cn}(u_{3\beta}, k_3) + n \cdot k_3 \operatorname{sn}(u_{3\beta}, k_3);$$

$$n' = -m \cdot k_3 + n \cdot k_3';\ k_3 = \operatorname{sn}(u_{3\theta}, k_{3\theta});\ k_3' = \operatorname{cn}(u_{3\theta}, k_{3\theta});\ k_3^2 + k_3'^2 = 1. \quad (9)$$

Here the dimensionless displacement $u_{3\beta}$ is connected with the polar angle $\varphi_{3\beta}$ in the plane Omj by relation $u_{3\beta} = F(\varphi_{3\beta}, k_3)$; the dimensionless displacement $u_{3\theta}$ is connected with the effective angle θ_3 by relation $u_{3\theta} = F(\theta_3, k_{3\theta})$; $k_3, k_{3\theta}$ are modules of elliptic functions.

Note that the formulas for the spatial rotations for cases when $k_{2\theta} = 0$, $k_{2\theta} = 1$ from (8) and $k_{3\theta} = 0$, $k_{3\theta} = 1$ from (9) are written by analogy as the expressions (4) - (7) with the parameters $n_{\theta 2}$ and $n_{\theta 3}$, respectively.

Earlier in the works [10, 11] the location of the singular points (attractors) of the deformation field in the core of fractal structures is typical for linear dislocation, real ellipse, hyperbola or an imaginary ellipse. In this paper, the singular points are located on fractal quasi-two-dimensional surfaces whose equations depend on three arguments n', m', j'. If in expressions (5) we put $\varphi_{1\beta} = 0$ for even values $n_{\theta 1} = 0; \pm 2; \ldots$, then $n' = n$, $m' = m$, $j' = j$, then the coordinate system $On'm'j'$ coincides with the original one $Onmj$.This allows us to

classify the original fractal structures (see table). In the table the sign «+» indicates a positive value of the parameter, the sign «$\pm$» indicates that the value of the parameter can be either positive or negative. Values of the parameters $p_1' \neq 0$, $p_2' \neq 0$, $p_3' \neq 0$ lead to the appearance of other fractal bulk structures. Further use of parameters $\varphi_{1\beta} \neq 0$ and $k_1 \neq 0$ allows performing investigations of the alteration of states of these fractal structures. Fig. 1 shows an example behavior of the displacement function u for the original fractal volumetric structure type of the fractal ellipsoid (FE) for the following parameters: $p_0' = 1.0123$; $u_{1\beta} = 0$; $u_{1\theta} = 0$; $k_{1\theta} = 0$ and the layer number in the multilayer nanosystem $j = 1, 19, 30, 44, 67$.

Table. Classification of the original fractal volumetric structures

Title of the fractal volumetric structure	p_0'	p_1'	p_2'	p_3'	b_1	b_2	b_3
Fractal ellipsoid (FE)	+	0	0	0	1	1	1
Fractal one-sheet hyperboloid (FOH)	+	0	0	0	1	1	-1
Fractal two-sheet hyperboloid (FTH)	+	0	0	0	1	-1	-1
Fractal elliptic cylinder (FEC)	+	0	0	0	1	1	0
Fractal hyperbolic cylinder (FHC)	+	0	0	0	1	-1	0
Fractal elliptic paraboloid (FEP)	+	0	0	$\pm$	1	1	0
Fractal hyperbolic paraboloid (FHP)	+	0	0	$\pm$	1	-1	0
Fractal quantum dot (FQD)	+	0	0	0	-1	-1	-1
Fractal stochastic state (FSS)	+	0	0	0	0	0	0

The solution of the nonlinear equation (1) with the value of function Q in the form (2) is obtained by the iterations method for fixed values $\alpha = 0.5$; $k = 0.5$; $u_0 = 29.537$. The iterative procedure on the index m simulates a stochastic process on a rectangular discrete lattice with size $N_1 \times N_2 = 30 \times 40$. The initial parameters were the following: $n_0 = 14.3267$; $n_c = 9.4793$; $m_0 = 19.1471$; $m_c = 14.7295$; $j_0 = 31.5279$; $j_c = 11.8247$.

Displacement function u for the boundary layers $j = 1$ and $j = 67$ is smooth with the maximum values $u = 4.2 \cdot 10^{-4}$ (Fig. 1a) and $u = 2.8 \cdot 10^{-4}$ (Fig. 1f) near the node $(n, m) = (n_0, m_0)$, respectively. As the number increases $j > 1$ at first there is the amplitude growth u. On the background of regular behavior of structures inside the elliptic region with semiaxes $n_c'(19) < n_c$, $m_c'(19) < m_c$ for $j = 19$ (Fig. 1b,g), there is a strongly pronounced stochastic behavior. Maximal amplitudes of displacement nodes are achieved near $j = j_0$. In this case the dislocation core (singular points) with a pronounced stochastic behavior is located on the ellipse with semiaxes $n_c'(30) \approx n_c$, $m_c'(30) \approx m_c$ (Fig. 1c,h). Within this region there is the inclined elliptical strip structure with

steps. With further increase of j decrease of amplitudes u takes place. Into an elliptical area with semiaxes $n_c'(44) < n_c$, $m_c'(44) < m_c$ for $j = 44$ (Fig. 1d,i), another strongly pronounced stochastic behavior compared to (Fig. 1b,g) appears. Further increase j leads to a decrease in amplitude and a change in curvature of the surface (Fig. 1e) as compared to the curvature of the surface (Fig. 1a,f). Note that the selected values of layers $j = 19 \approx j_0 - j_c$ and $j = 44 \approx j_0 + j_c$ correspond to transitions from regular to stochastic and from stochastic to the regular behavior of the deformation field, respectively. The layer $j = 30$ is located near the plane $j = j_0$.

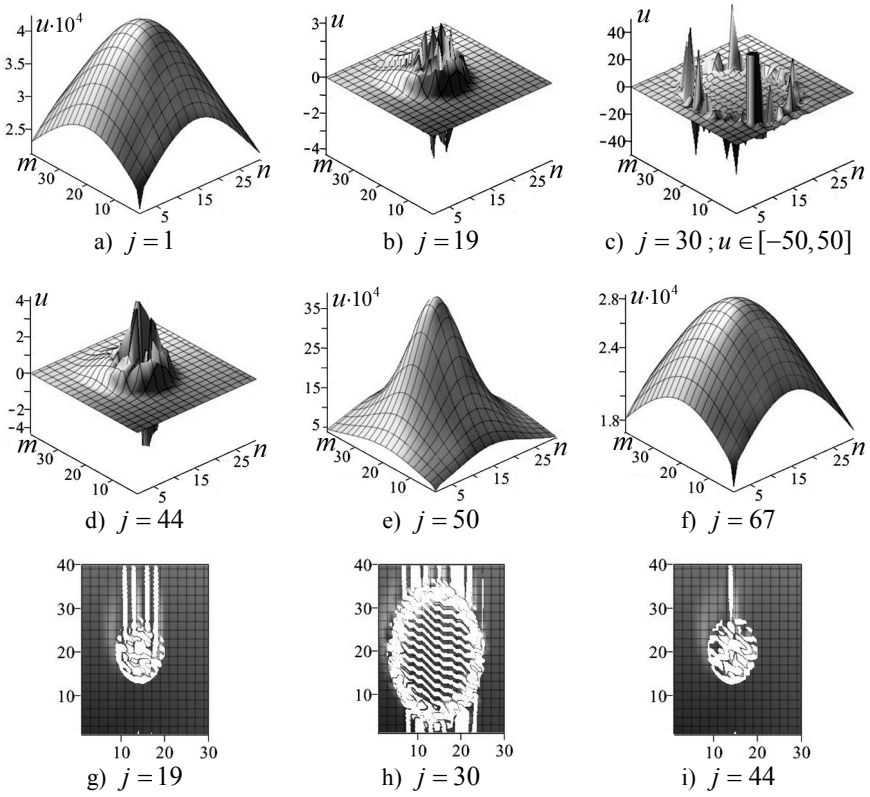

Fig. 1. Dependencies of the displacement function u (a-f) and cuts $u \in [0,1]$ (g-i, top view) on the lattice indexes n, m original structure FE for different j.

Original fractal structures, which rotations are described by (3), (8), (9) for $\varphi_{1\beta} = \varphi_{2\beta} = \varphi_{3\beta} = 0$ and $k_1 = k_2 = k_3 = 0$ coincide.

3. External and internal governance of the structure

An example of alteration structure that cuts fractal ellipsoid (FE) through various spatial rotations (external control) for layer $j = 30$ is shown in Fig. 2. The spatial rotation around the axis Oj (Fig. 2 a,b,c) is described by formulas (3). The spatial rotation around the axis Om (Fig. 2 d,e,f) is described by formulas (8). The spatial rotation around the axis On (Fig. 2 g,h,i) is described by formulas (9). Here the parameters of rotations and displacements are the following. The first alteration mechanism: the initial displacements are not zero $u_{1\beta} = u_{2\beta} = u_{3\beta} = -\pi / 8$, the effective angles are equal to zero $\theta_1 = \theta_2 = \theta_3 = 0$ (Fig. 2 a, d, g). The second alteration mechanism: the initial displacements are equal to zero $u_{1\beta} = u_{2\beta} = u_{3\beta} = 0$, the effective angles are not zero $\theta_1 = \theta_2 = \theta_3 = \pi / 16$ (Fig. 2 b,e,h). The third alteration mechanism: the initial displacements are not zero $u_{1\beta} = u_{2\beta} = u_{3\beta} = -\pi / 8$ and the effective angles are not zero $\theta_1 = \theta_2 = \theta_3 = \pi / 16$ (Fig. 2 c,f,i).

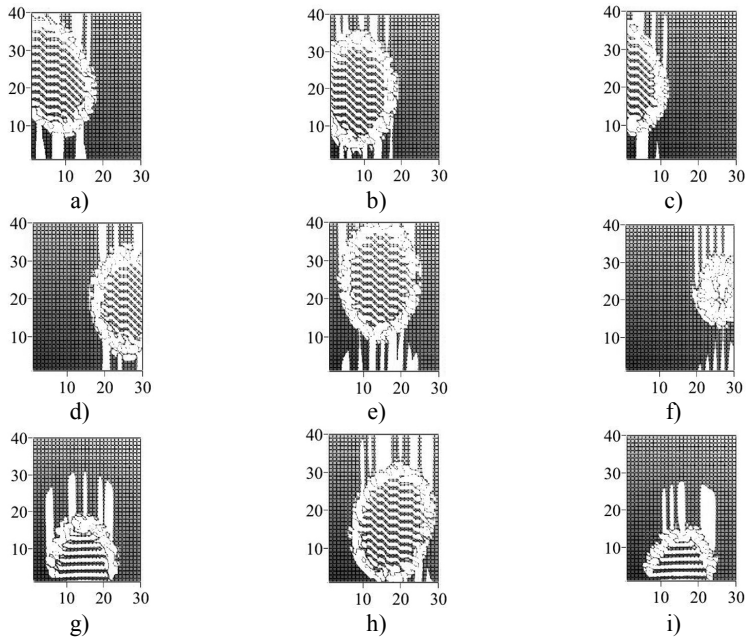

Fig. 2. Dependencies cuts of the displacement function $u \in [0,1]$ (top view) on n, m structure FE for the rotation around axes Oj (a, b, c), Om (d, e, f), On (g, h, i); $j = 30$.

A comparative analysis of Fig. 1h and Fig. 2 confirms the possibility of realization various alteration mechanisms of the fractal ellipsoid structure.

To investigate the behavior of the stochastic deformation field of fractal volumetric structures in multilayer nanosystem in terms of the statistical approach, averaged functions are introduced by analogy with paper [10].
The necessity of averaging is connected with the fact that the elements of the lattice nodes displacement matrix are in general case random real functions.
In the case of averaging over the nodes in a plane rectangular discrete lattice $N_1 \times N_2$ the operators fields of displacement $\hat{u}_1$ and density of states $\hat{\rho}_1$ are introduced. These operators are coincided to the rectangular matrix $\hat{u}_1$ and $\hat{\rho}_1$ with dimensions $N_1 \times N_2$ and $N_2 \times N_1$, matrix elements u_{nm} and $\rho_{mn} = 1 / N_2 N_1$, respectively.
In the case of averaging over the nodes in a plane $N_2 \times N_3$ the operators fields of displacement $\hat{u}_2$ and density of states $\hat{\rho}_2$ with dimensions $N_2 \times N_3$ and $N_3 \times N_2$, matrix elements u_{mj} and $\rho_{jm} = 1 / N_3 N_2$, respectively, are introduced.
In the case of averaging over the nodes in a plane $N_3 \times N_1$ the operators fields of displacement $\hat{u}_3$ and density of states $\hat{\rho}_3$ with dimensions $N_3 \times N_1$ and $N_1 \times N_3$, matrix elements u_{jn} and $\rho_{nj} = 1 / N_1 N_3$, respectively, are introduced. For a homogeneous distribution operators $\hat{\rho}_1, \hat{\rho}_2, \hat{\rho}_3$ are given by

$$\hat{\rho}_1 = \hat{\xi}_{N2}^T \hat{\xi}_{N1} / N_2 N_1; \quad \hat{\rho}_2 = \hat{\xi}_{N3}^T \hat{\xi}_{N2} / N_3 N_2; \quad \hat{\rho}_3 = \hat{\xi}_{N1}^T \hat{\xi}_{N3} / N_1 N_3. \quad (10)$$

where «T» denotes transposition; $\hat{\xi}_{N1}$, $\hat{\xi}_{N2}$, $\hat{\xi}_{N3}$ are row-vectors with elements equal to one. Averaged functions M_1, M_2, M_3 have the form

$$M_1(j) = Sp(\hat{\rho}_1 \hat{u}_1); \quad M_2(n) = Sp(\hat{\rho}_2 \hat{u}_2); \quad M_3(m) = Sp(\hat{\rho}_3 \hat{u}_3). \quad (11)$$

Here Sp is an operation of calculating the trace of a square matrix.
The behavior of averaged functions $M = M_1$ on j for $k_{1\theta} = 0$ without taking into account from the process of self-organization ($u_{1\beta} = 0$, $u_{1\theta} = 0$) is shown in Fig. 3 a,d. In this case for the specific layer j the matrix $\hat{u}_1$ with elements u_{nm} is filled in rows (for iteration m) or columns (for iteration n).
Inside the range $j \in (19;44)$ the stochastic behavior and the main peak down at $j = 40$ with values $M_1 = -20.0807$ (Fig. 3 a) and $M_1 = -3.1498$ (Fig. 3d) are observed. The comparison of the behavior of the averaged functions $M = M_1$ (Fig. 3 a,d) shows that the choice of the iterative procedure (either on m, either on n) leads to various stochastic processes.
This makes it possible to realize the stochastic governance of the alteration of

the structure. The behavior of the averaged function (Fig. 3 a) agrees with behavior of the displacement function of Fig. 1. Further taking into account the process of simple self-organization type of $u_{1\beta} = u$, $u_{1\theta} = 0$ (Fig. 3 b,e) or type of $u_{1\beta} = 0$, $u_{1\theta} = u$ (Fig. 3 c,f), respectively, leads to significant changes in the behavior of functions M_1 within the specified intervals.

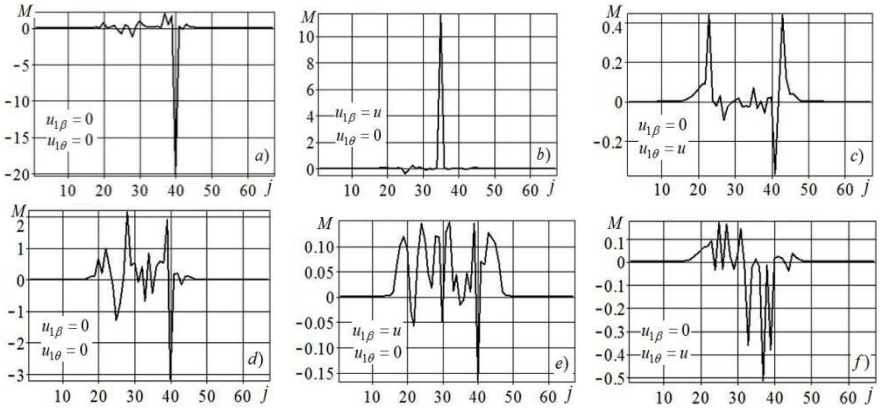

Fig. 3. The behavior of functions $M = M_1$ on j accounting for the process of simple self-organization for $k_{1\theta} = 0$: iteration on m (a, b, c); iteration on n (d, e, f).

Accounting for related processes (for effective displacement $u_{1\beta}$ and $u_{1\theta}$ through u) the self-organization of type $u_{1\beta} = \chi_{1\beta} u$, $u_{1\theta} = u$ (Fig. 4) leads to a further change in the behavior of the stochastic structure within the interval $j \in (19;44)$. The coefficient $\chi_{1\beta}$ can be interpreted as a compression factor ($\chi_{1\beta} < 1$) or extension factor ($\chi_{1\beta} > 1$) for the function u.

Accounting for the shift ($u'_{1\beta} \neq 0, u'_{1\theta} \neq 0$) for the effective displacement $u_{1\beta}$, $u_{1\theta}$ in the process of the related self-organization (Fig. 5) leads to significant changes in the behavior of the function M_1 compared with the behavior on Fig. 4 b. For the related self-organization of type $u_{1\beta} = u - u'_{1\beta}$, $u_{1\theta} = u$ (Fig. 5 a, b, c) within the interval $j \in (19;44)$ there is a change of the stochastic behavior to the regular one when parameter $u'_{1\beta}$ is being varied. The maximum of the function M_1 is near $j = j_0$ (Fig. 5 c). For the related self-organization of type $u_{1\beta} = u$, $u_{1\theta} = u - u'_{1\theta}$ (Fig. 5 d,e,f) when changing parameter $u'_{1\theta}$ the interval stochastic behavior shifts and further stochastic behavior is changed to regular. In this case the maximum of the function M_1 is near $j = j_c$ (Fig. 5 f).

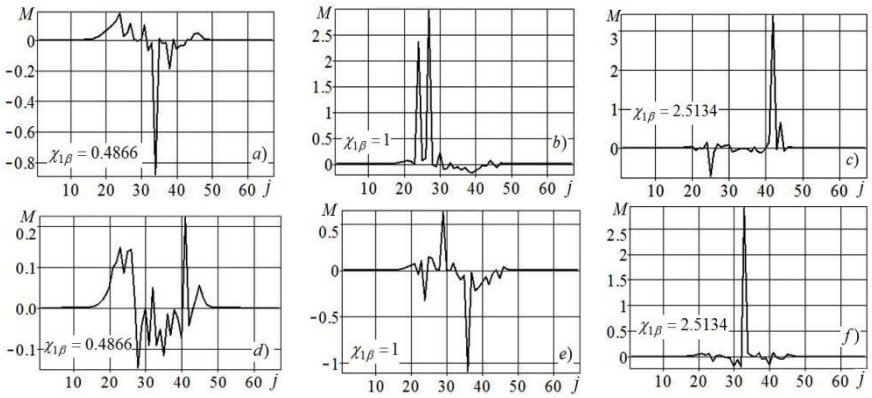

Fig. 4. The behavior of functions $M = M_1$ on j accounting for the process of related self-organization of type $u_{1\theta} = u$, $u_{1\beta} = \chi_{1\beta} u$ for $k_{1\theta} = 0$: iteration on m (a, b, c); iteration on n (d, e, f).

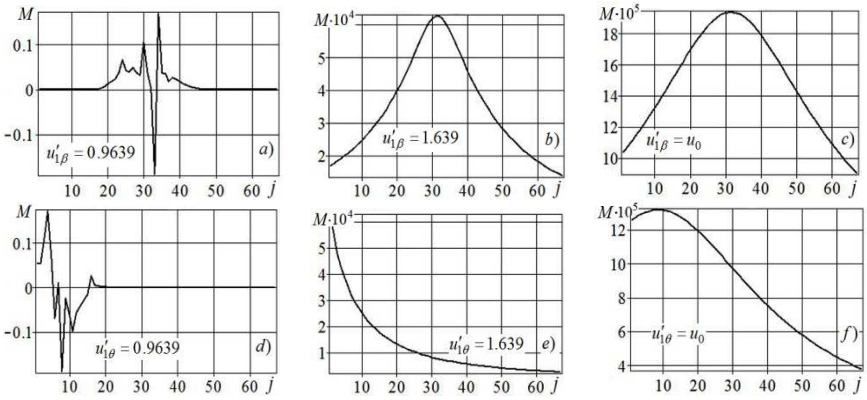

Fig. 5. The behavior of functions $M = M_1$ on j accounting for the process of related self-organization with shift for $k_{1\theta} = 0$: $u_{1\beta} = u - u'_{1\beta}$, $u_{1\theta} = u$ (a, b, c); $u_{1\beta} = u$, $u_{1\theta} = u - u'_{1\theta}$ (d, e, f). Iteration on m.

4. Conclusions

The iterative nonlinear equations for a multilayer nanosystem are obtained. These equations take into account the interaction of nodes both in the plane of the basic rectangular discrete lattices and the interplanar interactions. In this case, the fractal volumetric structures are formed, for which singular points are located on the core structure of fractal surfaces. On an example of volumetric

structure of type fractal ellipsoid (FE) the possibility of alteration of the deformation field states in the multilayer nanosystem using various spatial rotation (external control) is shown. Averaged functions for the averages in three main planes are introduced. The analysis of various types of internal governance of the structure is made. So for example, the possibility of FE stochastic governance of the structure due to the choice of the iterative process is shown. Also the internal governance of the structure through various processes of self-organization (simple, related, with a shift) is considered. Features of the behavior of averaged functions make it possible to determine the conditions of transition from one structure to another, and the characteristic parameters.

References

1. S. Gleyzes, S. Kuhr, C. Guerlin, et all. Quantum jumps of light recording the birth and death of a photon in a cavity. *Nature* **446**: 297-300, 2007.
2. C.W. Chou, D.B. Hume, T. Rosenband, et all. Optical clocks and relativity. *Science* **329**: 1630-1633, 2010.
3. K.V. Raman, A.M. Kamerbeek, A. Mukherjee. Interface-engineered templates for molecular spin memory devices. *Nature* **493**, 7433: 509-513, 2013.
4. S. Kahra, G. Leschhorn, M. Kowalewski. A molecular conveyor belt by controlled delivery of single molecules into ultrashort laser pulses. *Nature Physics* **8**, 3: 238-242, 2012.
5. Jan Awrejcewicz, V.A. Krysko. *Chaos in Structural Mechanics*. Springer-Verlag Berlin Heidelberg, 2008.
6. H.-J. Stockmann. *Quantum Chaos.An Introduction*. Cambridge Univers. Press, 1999.
7. C.H. Skiadas, C. Skiadas. *Chaotic Modeling and Simulation: Analysis of Chaotic Models, Attractors and Forms*. Taylor and Francis/CRC, London, 2009.
8. M.V. Zakrzhevsky, R.S. Smirnova, I.T. Schukin, et all. *Nonlinear dynamics and chaos. Bifurcation groups and rare attractors*. Riga, RTU, Publishing House, 2012.
9. V.S. Abramov. Fractal dislocation as one of non-classical structural objects in the nano-dimensional systems. *Metallofiz. i Noveishie Tekhnologii*. **33,** 2: 247-251, 2011.
10. O.P. Abramova, S.V. Abramov. Features of behaviour of the deformation field of fractal quasi-two-dimensional structures. *Bul. of Donetsk Nat. Univers.* Ser. **A,** 1: 9-17, 2013.
11. O.P. Abramova, S.V Abramov. Governance of Alteration of the Deformation Field of Fractal Quasi-two-dimensional Structures in Nanosystems. *Chaotic Modeling and Simulation (CMSIM) Journal*. **3**: 367-375, 2013.
12. O.P. Abramova, S.V Abramov. Fractal nanotraps based on quasi-two-dimensional fractal structures. *Dynamical Systems Theory* (Editors J.Awrejcewicz et. all.) DSTA 2013, Lodz, December 2-5, Poland: 71-80, 2013.
13. V.S. Abramov. Correlation Relations and Statistical Properties of the Deformation Field of Fractal Dislocation in a Model Nanosystem. *Chaotic Modeling and Simulation (CMSIM) Journal*. **3**: 357-365, 2013.

Transient Processes in a Model Multilayer Nanosystem with Nonlinear Fractal Oscillator

Valeriy S. Abramov

Donetsk Institute for Physics and Engineering named after A.A. Galkin,
National Academy of Sciences of Ukraine
E-mail: vsabramov@mail.ru

Abstract: Within the framework of the two-point model the states of deformation and stress fields of a fractal quantum dot, the stochastic state of discrete lattice in a model multilayer nanosystem are investigated. This uses the theory of fractional calculus and the concept of fractal. Accounting for the effect of bifurcation of solutions of nonlinear equations leads to the appearance of four branches of the lattice nodes displacement function. The numerical modelling of the complex deformation field behaviour is fulfilled on a rectangular discrete lattice. It is shown that for inverse (with a negative fractal index) states of nonlinear fractal oscillator there is an interval of change of this index with anomalous behaviour of the deformation field: there is no effective attenuation within the interval. The possibility of appearance of different transition effects such as induction, avalanches, supernutation, echo in the model multilayer nanosystem with nonlinear fractal oscillator is shown.
Keywords: fractal quantum dot, stochastic state of discrete lattice, deformation and stress fields, inverse states of fractal oscillator, model multilayer nanosystem.

1. Introduction

The actuality of fundamental research of individual quantum systems [1-9] is related to the possible use of them in quantum information technology [2-4]. As the information carrier (units, bits) the quanta of light – photons [1] are used. The recording and subsequent reading of quantum information (encoded in the polarization states of photons) are carried out on quantum states of single atoms or collective quantum states of the atomic ensemble. In the theoretical model description the main object is a qubit – two-level quantum system [5]. In the study of spontaneous parametric scattering, correlations and entanglement in quantum states of the system other model objects of types qutrit and ququarts [6] – the number of quantum systems with more than two levels – have been used. The quanta of vibrational excitations of the lattice – phonons, fractons [7] – can be used as another media. There are various mechanisms of relations and mutual transformations of some information carriers (photons) into others (phonons) in active nanostructured elements of quantum systems [8]. In [2] the behavior of the Fermi gas of ultracool atoms ^{40}K, trapped in an optical trap is studied. The existence of Dirac points when changing the lattice anisotropy and minimum energy gap within the Brillouin zone is shown. In [3] the Dirac fermions and topological phase in molecular graphene are studied. Near singular points Dirac fermions in molecular graphene show quantum and statistical features of behavior. In [9] the interaction of a single localized electron with Bose-Einstein condensate has been studied. It was shown that this electron can excite phonons and collective oscillations of all condensation. Individual

7th CHAOS Conference Proceedings, 7-10 June 2014, Lisbon Portugal
C. H. Skiadas (Ed)

quantum systems are also intensively studied on the base of organic semiconductors for the purpose of their application in quantum electronics, optics, spin information technology (spintronics). So, in [4] by the spin echo method the system of spin quantum qubits based on copper (CuP_c – cupper phthalocyanine) in organic films is studied. Physical properties of the arising transient processes of a spin type induction, echo were studied. Physical properties of these quantum systems (nanosystems) are essentially nonlinear. The methods of nonlinear dynamics have been applied to the theoretical description of the chaos [10] in structural mechanics [11], the analysis of nonlinear chaotic models [12], rare attractors and nonlinear oscillators [13]. In [14] it is proposed to use fractal nanotraps to capture individual particles or groups of particles in order to study their physical properties. At the same time it becomes necessary to conduct experimental and theoretical study of the properties of fractal quasi-two-dimensional and volumetric structures in the model multilayer nanosystems. In [14-20], the models of fractal dislocation [15-18] and fractal quasi-two-dimensional structures were considered as active elements in nanosystems [19]. In order to describe possible correlation effects and statistical properties of the deformation field of fractal dislocation a two-point model was proposed [18]. At excess of critical parameter values there are possible effects of bifurcation [17] solutions – the appearance of several branches in the energy spectrum. From the analysis of the behavior of the correlation functions of the first and second order on the dimensionless time the possibility of transition effects such as induction, avalanches, self-induced transparency, echo, effects of supernutation and propagation of linear fractal dislocation is shown [8].

The aim of this article is to study the deformation fields (after the bifurcation of solutions) of the fractal quantum dot, stochastic discrete lattice state, transient processes in model multilayer nanosystem with nonlinear fractal oscillator.

2. Nonlinear fractal oscillator in nanosystem

At construction of model of fractal dislocation in the [14-20] the Hamilton operator $\hat{H}_2$ from [15, 20] was used for the energy spectrum of fractal dislocation

$$\hat{H}_2 = \varepsilon_1\hat{n}_1 + \varepsilon_2\hat{n}_2 + \varepsilon_3\hat{n}_3';\ \hat{n}_1 = \hat{a}_1^+\hat{a}_1;\ \hat{n}_2 = \hat{a}_2^+\hat{a}_2;\quad \hat{n}_3' = \hat{a}_3\hat{a}_{\mathbf{3}}^+;\ \hat{n}_3 = \hat{a}_{\mathbf{3}}^+\hat{a}_3. \quad (1)$$

$$\hat{H}_2 = \hat{H}_1 + b_0\hat{b}_{\alpha 3};\quad \hat{H}_1 = \varepsilon_2(\hat{n}_1 + \hat{n}_2) + \varepsilon_3\hat{n}_3.$$

Here $\hat{n}_1, \hat{n}_2, \hat{n}_3$ are the operators of occupation numbers of states of dislocation with non-dimensional own energies $\varepsilon_1 = \varepsilon_2, \varepsilon_3$. The relations between the new $\hat{a}_1^+, \hat{a}_2^+, \hat{a}_3$ and old $\hat{\psi}_1, \hat{c}^+, \hat{c}$ operators are defined by expressions

$$\hat{a}_1^+ = t_{11}\hat{\psi}_1 + t_{21}\hat{c}^+ + t_{31}\hat{c};\ \hat{a}_2^+ = t_{12}\hat{\psi}_1 + t_{22}\hat{c}^+ + t_{32}\hat{c};\ \hat{a}_3 = t_{23}\hat{c}^+ + t_{33}\hat{c};\ \hat{\psi}_1 = D_z^{\alpha}. \quad (2)$$

In expressions (2) the elements t_{ij} of the matrix $\hat{T}$ are defined by the relations

$$t_{11} = k';\quad t_{12} = -k;\quad t_{13} = 0;\quad t_{21} = k\,cn(u_\alpha, k);\quad t_{22} = k'\,cn(u_\alpha, k);$$

$$t_{23} = -sn(u_\alpha, k);\quad t_{31} = k\,sn(u_\alpha, k);\quad t_{32} = k'sn(u_\alpha, k);\quad t_{33} = cn(u_\alpha, k). \quad (3)$$

Here k and $u_\alpha = F(\varphi_\alpha, k)$ are the module and the argument of the Jacobi

elliptic functions $sn(u_\alpha,k)$, $cn(u_\alpha,k)$; $(k')^2=1-k^2$; F is an incomplete elliptic integral of the first kind; φ_α is the polar angle. Using (2), we find the commutation relations for the new operators

$$[\hat{a}_3,\hat{a}_3^+]=\hat{n}_3'-\hat{n}_3=b_0\hat{b}_{\alpha 3}\ ;\ \ b_0=1-2n_{30}\ ;\ \ n_{30}=sn^2(u_\alpha,k)\,;$$

$$\hat{b}_{\alpha 3}=[\hat{\psi}_2,\hat{z}]=(1-\alpha)I_z^\alpha=[\hat{c},\hat{c}^+]\ ;\ \ \hat{\psi}_2=D_z^{1-\alpha}\ ;\ \ \hat{b}_{\alpha 2}=[\hat{\psi}_1,\hat{z}]=\alpha I_z^{1-\alpha}\,, \quad (4)$$

where $\hat{z}$ is the coordinate operator. The structure of operators of fractional partial derivative (integral) of the Riemann-Liouville D_z^α (I_z^α) on dimensionless coordinate z with the index order α is defined as

$$D_z^\alpha\Phi=\partial_z\int_{z_0}^z\Phi(\xi)\,|z-\xi|^{-\alpha}\,d\xi/\Gamma(1-\alpha)\,,\quad I_z^\alpha\Phi=\int_{z_0}^z\Phi(\xi)\,|z-\xi|^{\alpha-1}\,d\xi/\Gamma(\alpha)\,, \quad (5)$$

where ∂_z is the operator of ordinary partial derivative on z; Γ is gamma function. Indices $\alpha, 1-\alpha$ have the meaning of fractal dimensions along the axis Oz. Acting by the operator $\{\hat{c},\hat{c}^+\}=\hat{c}\hat{c}^++\hat{c}^+\hat{c}=\hat{z}^2-\hat{\psi}_2^2$ to the function $\Phi_{\alpha c}$, we obtain the equation a fractal oscillator

$$(\hat{z}^2-\hat{\psi}_2^2)\Phi_{\alpha c}=(\hat{z}^2-D_z^{1-\alpha}D_z^{1-\alpha})\Phi_{\alpha c}=(\hat{c}\hat{c}^++\hat{c}^+\hat{c})\Phi_{\alpha c}=(2n_{\alpha c}+1)\Phi_{\alpha c}\,. \quad (6)$$

Here $n_{\alpha c}$, $\Phi_{\alpha c}$ are the eigenvalues (generally fractional values, may depend on z, α), eigenfunctions of the fractal oscillator. Acting by the operator $D_z^\alpha\hat{b}_{\alpha 3}$ on the left to the function $\Phi_{\alpha c}$, we obtain the nonlinear equation

$$D_z^\alpha\hat{b}_{\alpha 3}\Phi_{\alpha c}=D_z^\alpha[\hat{c},\hat{c}^+]\Phi_{\alpha c}=(1-\alpha)\Phi_{\alpha c}\,. \quad (7)$$

To find the eigenvalues $n_{\alpha c}$ and eigenfunctions $\Phi_{\alpha c}$ the equations (6), (7) must be solved together. These equations are fundamental to describe the nonlinear fractional oscillator. Dimensionless displacement u of points of fractal dislocation (deformation field) is connected with a parameter λ_α (stress field) by model relations (Hooke's law) $u=\lambda_\alpha/\lambda_0=F(\varphi,k)$, $u_\alpha=u-u_0$, where λ_0 is the normalization parameter; u_0 is the constant (critical) displacement.

In this two-point model [18] based on the Hamiltonian $\hat{H}_2$ (1) the deformation fields of the stochastic discrete lattice state, the fractal quantum dot in a model sample of finite nanosize with volumetric discrete lattice $N_1\times N_2\times N_3$ is investigated. The deviations of the lattice nodes from the state of equilibrium in a separate plane $N_1\times N_2$ for two different points of $z_1(j,j_z)$ and $z_2(j,j_z)$ are described by non-hermitian displacements operators $\hat{u}(z_1)$ and $\hat{u}(z_2)$, corresponding to the rectangular matrix with dimensions $N_1\times N_2$, $j\in[1,N_3]$. The value of j_z plays the role of dimensionless current discrete time [8, 20]. The original rectangular matrix displacement $\hat{u}(z_1)$ and $\hat{u}(z_2)$ with elements $u_{nm}(z_1)=u_{\varepsilon s}(z_1)$, $u_{nm}(z_2)=u_{\varepsilon s}(z_2)$ ($s=1,2,3,4$) in volumetric lattice $N_1\times N_2\times N_3=30\times 40\times 67$ were obtained by the method of iterations on an

index m for the four branches of the dimensionless complex displacement function by the formulas in [17, 20], respectively

$$u(z)=u_{\varepsilon 1}(z)=(g_1-g_2+g_4)/2;\quad u(z)=u_{\varepsilon 2}(z)=(g_1-g_2-g_4)/2;$$
$$u(z)=u_{\varepsilon 3}(z)=(-g_1-g_2+g_5)/2;\quad u(z)=u_{\varepsilon 4}(z)=(-g_1-g_2-g_5)/2. \quad (8)$$

Functions g_1, g_2, g_3, g_4, g_5 by analogy with [17, 20] are modeled by expressions

$$g_1(u,\alpha)=(1-\alpha)(1-2\,\mathrm{sn}^2(u-u_0,k))/Q; \quad (9)$$

$$g_2(z,\alpha)=2^{-2\alpha}3^{3\alpha-1/2}\,|z-z_c|^{-\alpha}\,\Gamma(\alpha+1/3)\Gamma(\alpha+2/3)/\sqrt{\pi}\,\Gamma(\alpha+1/2); \quad (10)$$

$$g_3(z,\alpha)=3^{3\alpha-1/2}\,2|z-z_c|^{-2\alpha}\,\Gamma(\alpha+1/3)\Gamma(\alpha+2/3)/\pi;$$
$$g_4=[(g_1+g_2)^2-g_3]^{1/2};\quad g_5=[(-g_1+g_2)^2-g_3]^{1/2}; \quad (11)$$

The initial expression for Q has the form

$$Q=p_0'+p_1'n+p_2'm+p_3'j-b_1\left(\frac{n'-n_0}{n_c}\right)^2-b_2\left(\frac{m'-m_0}{m_c}\right)^2-b_3\left(\frac{j'-j_0}{j_c}\right)^2. \quad (12)$$

The expression (12) has thirteen parameters. The parameter p_0' is independent of the variables n, m, j; parameters p_1', p_2', p_3' are included in the linear form; parameters b_1, b_2, b_3, n_0, n_c, m_0, m_c, j_0, j_c determine the behavior of the quadratic form. Parameters n_c, m_c, j_c play the role of semi-axes of fractal volumetric structures in a new coordinate system $O'n'm'j'$. The original coordinate system $Onmj$ is described in terms of variables n, m, j.

Performing spatial axis rotation of the coordinate system around axis Oj, we move from the system $Onmj$ to the system $O'n'm'j'$ by the formulas

$$n'=n\cdot k_1'\,\mathrm{cn}(u_{1\beta},k_1)-m\cdot\mathrm{sn}(u_{1\beta},k_1)+j\cdot k_1\,\mathrm{cn}(u_{1\beta},k_1);$$
$$m'=n\cdot k_1'\,\mathrm{sn}(u_{1\beta},k_1)+m\cdot\mathrm{cn}(u_{1\beta},k_1)+j\cdot k_1\,\mathrm{sn}(u_{1\beta},k_1);$$
$$j'=-n\cdot k_1+j\cdot k_1';\ k_1=\mathrm{sn}(u_{1\theta},k_{1\theta});\ k_1'=\mathrm{cn}(u_{1\theta},k_{1\theta});\ k_1^2+k_1'^2=1. \quad (13)$$

Here the dimensionless displacement $u_{1\beta}$ is connected with the polar angle $\varphi_{1\beta}$ in the plane Onm by relation $u_{1\beta}=F(\varphi_{1\beta},k_1)$; F is an incomplete elliptic integral of the first kind; the dimensionless displacement $u_{1\theta}$ is connected with the effective angle θ_1 by relation $u_{1\theta}=F(\theta_1,k_{1\theta})$; $k_1, k_{1\theta}$ are modules of elliptic functions. The dimensionless displacement $u_{1\beta}$ is a nonlinear function of two parameters $\varphi_{1\beta}$ and k_1, that define the different mechanisms of alteration of fractal volumetric structure and governing it. Here the parameter k_1 is a nonlinear function of $u_{1\theta}$ and $k_{1\theta}$. As a result, the displacement $u_{1\beta}$ becomes a complex function depending on three parameters

$\varphi_{1\beta}$, $u_{1\theta}$, $k_{1\theta}$.In the calculations it should be: $z_1 = 0.053 + h_z(j_z + 33)$; $z_2 = 6.653 - h_z(j_z + 33)$; $h_z = 0.1$, which corresponds to the forward and backward waves of displacements $u_{nm}(z_1)$, $u_{nm}(z_2)$; $n = \overline{1,30}$; $m = \overline{1,40}$. For $j_z = 0$ we have $z_1 = z_2 = 3.353$.

Averaged functions $M_{\varepsilon s}$ have the form [15, 16, 20]

$$M = M_{\varepsilon s}(j) = Sp(\hat{\rho}_1 \hat{u}_{\varepsilon s}) = M'_{\varepsilon s} + iM''_{\varepsilon s}; \quad \hat{\rho}_1 = \hat{\xi}^T_{N2}\hat{\xi}_{N1} / N_2 N_1. \quad (14)$$

Here Sp is an operation of calculating the trace of a square matrix; «T» denotes transposition; $\hat{\xi}_{N1}$, $\hat{\xi}_{N2}$ are row-vectors with elements equal to one; $M'_{\varepsilon s} = \mathrm{Re}(M_{\varepsilon s})$, $M''_{\varepsilon s} = \mathrm{Im}(M_{\varepsilon s})$.

3. Stochastic state of the multilayer nanosystem

For the investigation of transient processes in multilayer nanosistem with nonlinear fractal oscillator the initial parameters were as follows: $k = 0.5$; $u_0 = 29.537$; $n_0 = 14.3267$; $n_c = 9.4793$; $m_0 = 19.1471$; $m_c = 14.7295$; $j_0 = 31.5279$; $j_c = 11.8247$; $p'_1 = 0$; $p'_2 = 0$; $p'_3 = 0$. In modeling the stochastic state deformation field of volumetric lattice it was assumed: $p'_0 = 1.0123$; $b_1 = b_2 = b_3 = 0$. For a negative fractal index $\alpha = -0.5$ the behavior of four branches (8) of displacement function u for forward and backward waves is given in Fig. 1, 2. These results were obtained for variant with $u_{1\beta} = 0$; $u_{1\theta} = 0$; $k_{1\theta} = 0$. From (14) it follows that the spatial rotation of the coordinate system is missing: $n' = n$; $m' = m$; $j' = j$. It was also assumed that $j_z = j'$, therefore, the displacement function $u(z) = u(z(j, j_z)) = u(z(j, j')) = u(z(j, j)) = = w(j)$ becomes a function on j. Note that the imaginary part of the displacement u is zero for all four branches, which indicates the anomalous behavior of the inverse structural states (with negative indices $\alpha \in (-2/3; -1/3)$) of the deformation field. When $j = 5$ for the forward wave (Fig. 1a,b,c) the behavior of displacement function for all branches is regular: along the axis Om for branches 3, 4 oscillations are observed; for branches 1, 2 the output on constant values with increasing m is characteristic (Fig. 1c). For the backward wave (Fig. 1d,e,f) besides regular behavior of branches 1, 2, 3 the pronounced stochastic behavior of branch 4 is observed. Note that for backward wave parameter $|z_2 - z_c|$ from the expression (10), (11) has a minimum for $j = 5$, and the parameter $|z_1 - z_c|$ changes monotonically on j. Behavior projection displacement u as functions of m for various j of the backward wave (Fig. 2) clearly demonstrates the presence and features of transient processes (such as of structural alteration) in the model multilayer nanosystem. When $j_z = j' = j = 0$ (Fig. 2a) the displacement function for all branches of the backward and forward waves coincide. With

increasing j the behavior of branches for the forward and backward waves begins to differ (Fig. 1).

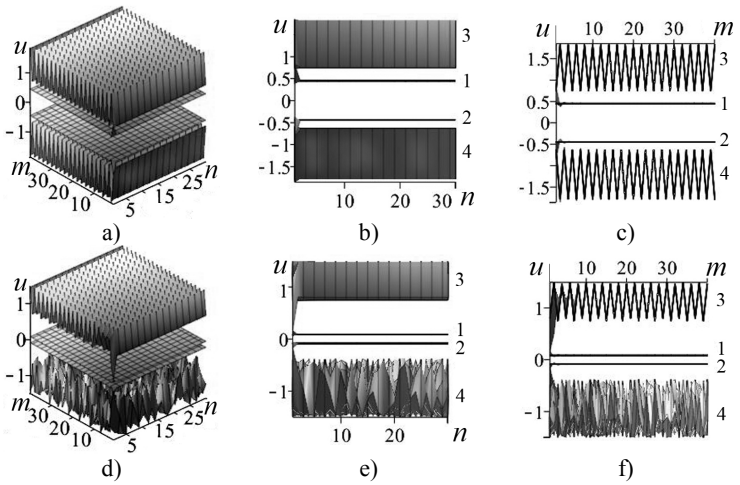

Fig. 1. Dependencies of the displacement function u and projections on planes nOu, mOu for forward (a, b, c) and backward (d, e, f) waves on the lattice indexes n, m: 1 – branch $u_{\varepsilon 1}$, 2 – branch $u_{\varepsilon 2}$, 3 – branch $u_{\varepsilon 3}$, 4 – branch $u_{\varepsilon 4}$; $j = 5$, $\alpha = -0.5$.

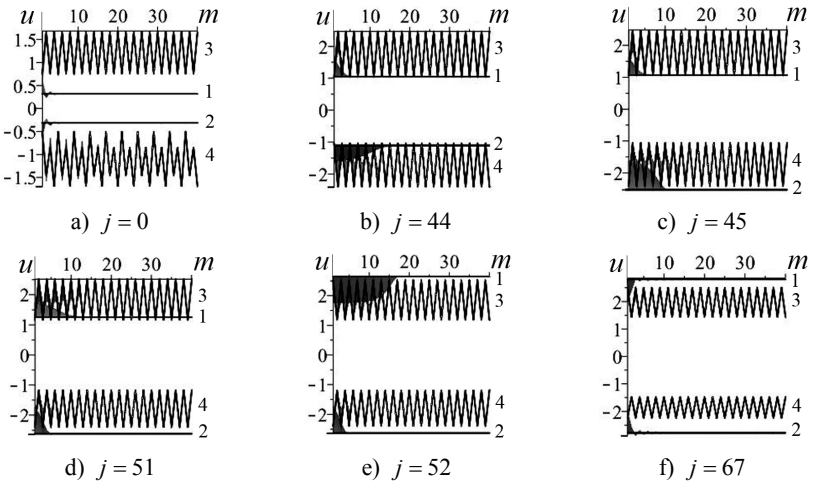

Fig. 2. Dependencies of the projections on plane mOu function u on m for different j: 1 – branch $u_{\varepsilon 1}$, 2 – branch $u_{\varepsilon 2}$, 3 – branch $u_{\varepsilon 3}$, 4 – branch $u_{\varepsilon 4}$; $\alpha = -0.5$, backward wave.

For backward wave the change of order of the branches is characteristic: for $j = 44$ (Fig. 2b) branch 2 is located above branch 4 and for $j = 45$ (Fig. 2c)

branch 2 becomes below branch 4; for $j = 51$ (Fig. 2d) branch 1 is located below branch 3 and for $j = 52$ (Fig. 2e) branch 1 becomes above branch 3. This behavior is confirmed by the intersection of the dependence of the average functions M for backward wave (Fig. 3b). For forward wave the crossing effect and the changing of location order branches of the displacement function for values $j = 33$, $j = 34$ and $j = 41$, $j = 42$ are confirmed by the dependencies of the average functions M (Fig. 3a).

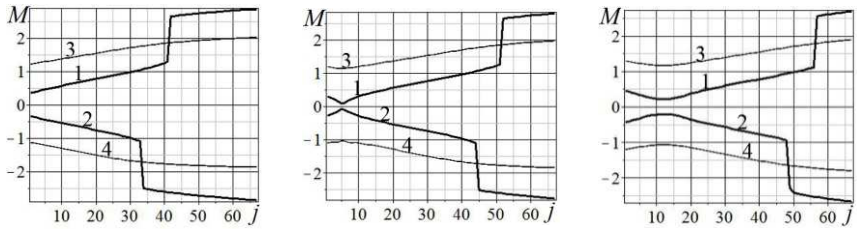

Fig. 3. Dependencies of functions M on j for four branches of displacement function u for forward (a) and backward (b) waves: curves 1, 2 (thick lines) - $M_{\varepsilon 1}$, $M_{\varepsilon 2}$; curves 3, 4 (thin lines) - $M_{\varepsilon 3}$, $M_{\varepsilon 4}$, respectively, $\alpha = -0.5$. Effect of rotation, backward wave (c).

On the dependencies of the average functions $M_{\varepsilon 1}$, $M_{\varepsilon 2}$ for forward and backward waves (Fig. 3a,b) there are features such as "inclined steps" that is characteristic of the hysteresis phenomena. For backward wave on the curves $M_{\varepsilon 1}$, $M_{\varepsilon 2}$, (Fig. 3b) for $j = 5$ the local minimum, maximum are also observed, respectively, which is typical for the type of behavior of the soft mode [20]. By choosing the parameters $u_{1\theta} = \pi / 8$, $k_{1\theta} = 1$, $u_{1\beta} = 0$ the rotation of the coordinate system is carried out. The influence of this rotation on the behavior of the averaged functions $M(j)$ for backward wave is given in Fig. 3c. Effects of shifting and broadening of the main features in comparison with Fig. 3b are observed. For values of the fractal index $\alpha \in (-1; -2/3)$ and $\alpha \in (-1/3; 1)$ all branches are characterized by the presence of both real and imaginary parts of the displacement function. For backward wave for $\alpha = 0.5$ the dependencies of the average complex functions are shown in Fig. 4. These results were obtained for the variant with parameters $u_{1\beta}$=0; $u_{1\theta}$=0; $k_{1\theta}$=0 (excluding the effect of rotation). For all branches the presence of their critical value $j = j_k$ is characteristic. Within the regions of changes $j \in [1; j_k]$ the behavior of functions is stochastic. On the dependencies $M'_{\varepsilon s}$, $M''_{\varepsilon s}$ of the dimensionless time $j_z = j' = j$ transient processes with the formation of complex shapes signals are observed, which allow the interpretation of the type of fractal induction, nutation, supernutation, echo, avalanches, self-induced transparency [7].

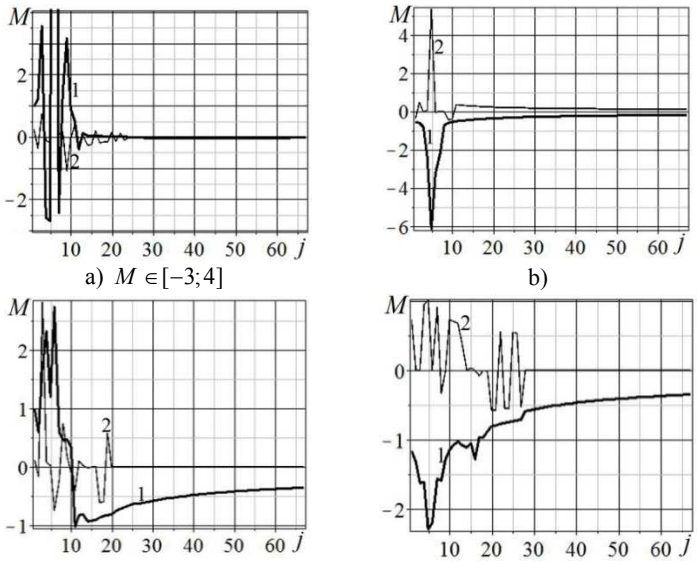

Fig. 4. Dependencies of M on j for four branches of u : a) $M_{\varepsilon 1} \in [-3;5]$; b) $M_{\varepsilon 2}$; c) $M_{\varepsilon 3}$; d) $M_{\varepsilon 4}$. Curve 1 (thick lines) - $M'_{\varepsilon s}$, curve 2 (thin lines) - $M''_{\varepsilon s}$; $\alpha = 0.5$, backward wave.

When $j > j_k$ the behavior of functions $M'_{\varepsilon s}(j)$, $M''_{\varepsilon s}(j)$ is almost regular with monotonic changes in the laws, close to power dependences. Note that the strongest changes of the averaged functions $M'_{\varepsilon s}(j)$, $M''_{\varepsilon s}(j)$ are observed near $j = 5$. At the same value j for inverse states with $\alpha = -0.5$ (Fig. 3) the behavior of the soft mode type is observed [20].

4. Quantum dot in multilayer nanosystem

For quantum dot the basic parameters were as follows: $p'_0 = -3.457 \cdot 10^{-11}$; $b_1 = b_2 = b_3 = 1$. Other parameters were the same as for the stochastic state. The choice of parameters corresponds to the location of the singular points of the deformation field on the fractal imaginary ellipsoid. First, we consider the state of a quantum dot with a fractal negative index $\alpha = -0.5$. On Fig. 5 there is an example of the behavior of the averaged functions M for the four branches (8) of forward (Fig. 5a) and backward (Fig. 5b) waves. These results have been obtained for the variant with $u_{1\beta} = 0$; $u_{1\theta} = 0$; $k_{1\theta} = 0$. On the dependencies $M_{\varepsilon 3}(j)$, $M_{\varepsilon 4}(j)$ of the forward and backward waves (Fig. 5a,b) such features as "blurry steps" are observed compared with features such as "inclined steps" on the curves $M_{\varepsilon 1}(j)$, $M_{\varepsilon 2}(j)$ from Fig. 3a,b. On the dependencies $M_{\varepsilon 1}(j)$, $M_{\varepsilon 2}(j)$ (Fig. 5a,b) peak up, peak down for $j = 31$ appear, respectively. For backward wave

for $j = 5$ at all four branches (Fig. 5b) local minima, maxima are additionally observed, which is typical for the behavior of the soft mode type [20].

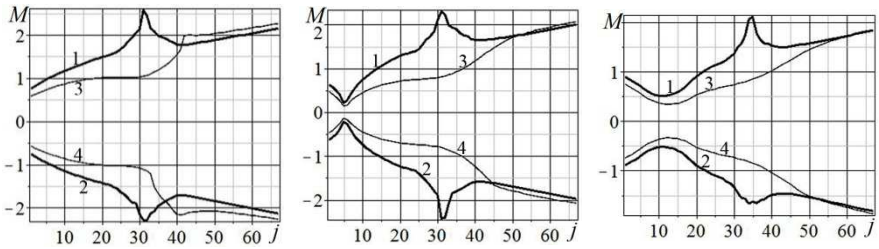

Fig. 5. Dependencies of M on j for four branches of u for forward (a) and backward (b) waves, $\alpha = -0.5$: curves 1, 2 (thick lines) - $M_{\varepsilon 1}$, $M_{\varepsilon 2}$; curves 3, 4 (thin lines) - $M_{\varepsilon 3}$, $M_{\varepsilon 4}$; effect of rotation for backward wave (c).

Between branches 1 and 3, 4 and 2 there is crossing of branches (Fig. 5a,b). By choosing the parameters $u_{1\theta} = \pi/8$, $k_{1\theta} = 1$, $u_{1\beta} = 0$ the rotation of the coordinate system is carried out. The influence of this rotation on the behavior of the averaged functions $M(j)$ for backward wave is given in Fig. 5c. The effects of shifting and broadening of the main features in comparison with Fig. 5b are observed. Below the behavior of the four branches (8) of displacement function u of forward wave for the characteristic values $j = 31$ (Fig. 6) and $j = 42$ (Fig. 7) is given. The imaginary part of the displacement function u for all branches is zero. For branch 1 (Fig. 6a) the presence of peak up localized near node (n_0, m_0) with a large amplitude and stochastic behavior in the quantum dot region (Fig. 6b) is characteristic. For branch 2 (Fig. 6c) a peak down is observed, which is also localized near the node (n_0, m_0) with other amplitude and stochastic behavior in the quantum dot region. For branch 3 (Fig. 6d) almost regular behavior with small positive amplitudes and minimum near the node (n_0, m_0) is observed. For branch 4 (Fig. 6e) almost regular behavior with small negative amplitudes and maximum near the node (n_0, m_0) is observed. On Fig. 6f the section $u \in [-2; 2]$ of all four branches together is given: branches 1 and 3 generally have positive values, 2 and 4 – negative. There is the crossing of the four branches of the displacement function at separate points. Between the branches of the displacement function gaps are observed. With an increase of j the behavior of all four branches of the displacement function changes (Fig. 7). This is due to the change $Q(j)$ (13) and the parameter $|z(j) - z_c|$ from expressions (10), (11) for four branches of the displacement function (8). The changes in the values of gaps between the branches of displacement function are also observed. Note that the behavior of

the four branches of the displacement function, the gaps between the branches, the location of the singular points are qualitatively similar to the behavior of the physical parameters close to the Dirac points [2, 3]. It is also possible to have the physical interpretation of the displacement function as a function of the dimensionless wave number $q_z = (z - z_c)/z_c$.

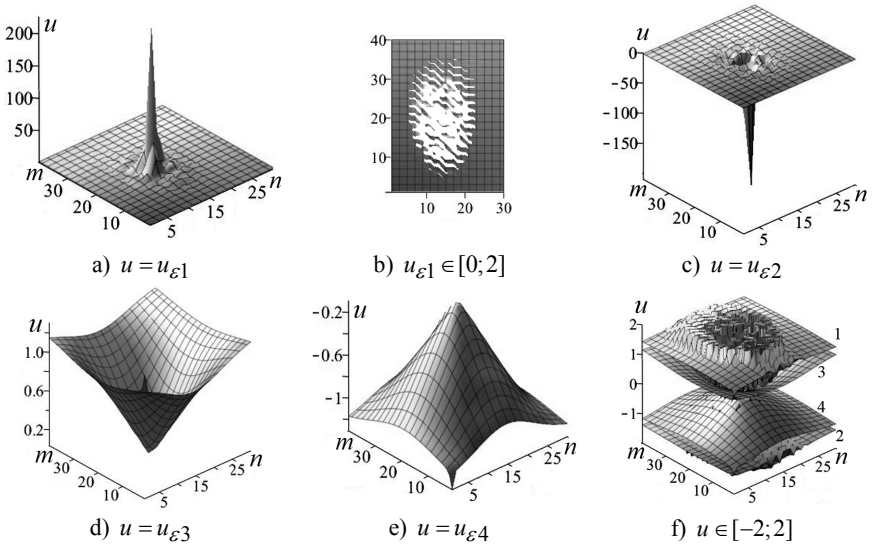

Fig. 6. Dependencies of u on the lattice indexes n, m for forward wave: (a) 1 – branch $u_{\varepsilon 1}$, (b) cut $u_{\varepsilon 1} \in [0;2]$ (top view), (c) 2 – branch $u_{\varepsilon 2}$, (d) 3 – branch $u_{\varepsilon 3}$, (e) 4 – branch $u_{\varepsilon 4}$, (f) dependences of the four branches; $j = 31$, $\alpha = -0.5$.

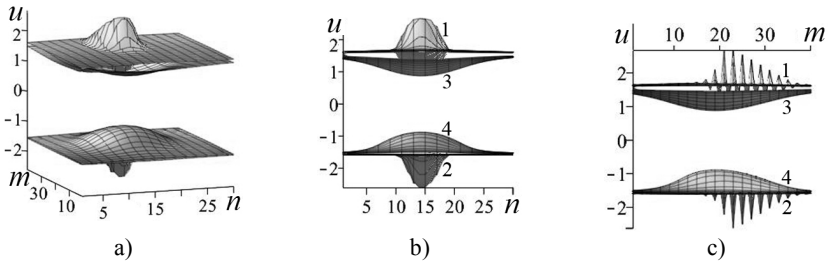

Fig. 7. Dependencies of u (a), the projections on planes nOu (b) and mOu (c) on the lattice indexes n, m for forward wave: 1 – branch $u_{\varepsilon 1}$, 2 – branch $u_{\varepsilon 2}$, 3 – branch $u_{\varepsilon 3}$, 4 – branch $u_{\varepsilon 4}$; $j = 42$, $\alpha = -0.5$.

When $\alpha = 0.5$ the displacement function u is complex. Each of the functions $M'_{\varepsilon s}$, $M''_{\varepsilon s}$ (Fig. 8) has the characteristic range of values $j \in (j_0 - j_{ks}; j_0 + j_{ks})$, within the behavior of these functions are very different. Here j_{ks} is some critical value.

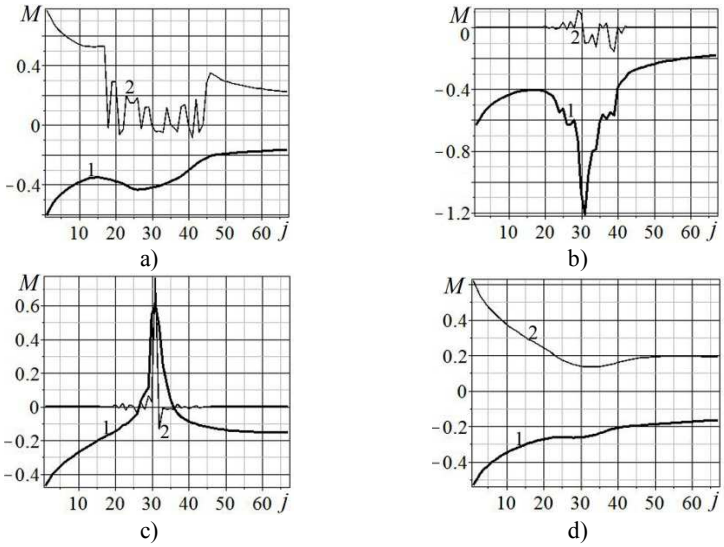

Fig. 8. Dependencies of M on j for four branches of u : a) $M_{\varepsilon 1}$; b) $M_{\varepsilon 2}$; c) $M_{\varepsilon 3}$; d) $M_{\varepsilon 4}$. Curve 1 (thick lines) - $M'_{\varepsilon s}$, curve 2 (thin lines) - $M''_{\varepsilon s}$; $\alpha = 0.5$, forward wave.

So functions $M''_{\varepsilon 1}$, $M''_{\varepsilon 2}$, $M''_{\varepsilon 3}$ within specific intervals have pronounced stochastic behavior, and the behavior of functions $M'_{\varepsilon 1}$, $M'_{\varepsilon 3}$, $M'_{\varepsilon 4}$, $M''_{\varepsilon 4}$ is almost regular. Function $M'_{\varepsilon 2}$ describes the formation of a signal with a complex shape. On dependencies $M'_{\varepsilon 2}$, $M'_{\varepsilon 3}$, $M''_{\varepsilon 2}$ near the value j_0 pronounced peaks are observed. The behavior of the functions (Fig. 8) demonstrates the possibility of the appearance of various transient processes in a model multilayer nanosystem with quantum dot. The analysis of these dependencies allows us to estimate the critical values j_{ks}, that are associated with the dimensionless relaxation times of each of the branches $u_{\varepsilon s}$ of the complex displacement function u. Outside characteristic intervals all functions practically change monotonous by its laws.

5. Conclusions

The behavior of the four branches of the complex displacement function on the dimensionless time for the stochastic state and the fractal quantum dot in model multilayer nanosystem is investigated. The appearance of four branches is connected with the bifurcation effect of solutions of nonlinear equations system for multilayer nanosystem with fractal oscillator. For values of the fractal index $\alpha \in (-1;-2/3)$ and $\alpha \in (-1/3;1)$ all branches are characterized by the presence of both real and imaginary parts of the displacement function. It is shown that changing the dimensionless time may cause transient effects such as fractal induction, nutation, supernutation, echo, avalanches, self-induced transparency. Within the range of variation of the fractal index $\alpha \in (-2/3;-1/3)$ the imaginary part of displacement function is zero for all four branches, which indicates the anomalous behavior of the inverse structural states. The analysis of

the behavior of the averaged functions and displacement functions allows to reveal features such as soft mode, "inclined steps", the presence of hysteresis, gaps between the branches of displacement function, the presence type of singular Dirac points. By increasing the dimensionless time the change of the structure of the displacement field of each of the four branches, the change of the gaps between the branches, the crossing of the branches in selected areas (transient processes type of structural alteration) take place.

References

1. M.O. Scully, M.S. Zubairy. *Quantum Optics.* Cambridge: Cambridge Univ. Press, 1997.
2. L. Tarruell, D. Greif, T. Uehlinger et. all. Greating, moving and merging Dirac points with a Fermi gas in a tunable honeycomb lattice. *Nature* **483,** 7389: 302-305, 2012.
3. K.K. Gomes, W. Mar, W. Ko et. al. Designer Dirac fermions and topological phases in molecular graphene. *Nature* **483,** 7389: 306-310, 2012.
4. M. Warner, S. Din, I. Tupitsyn et. all. Potential for spin-based information processing in a thin-film molecular semiconductor. *Nature* **503,** 7477: 504-508, 2013.
5. L. Allen, J.H. Eberly. *Optical Resonance and Two-level Atoms.* Wiley Interscience Publication, New York-London-Sydney-Toronto, 1975.
6. M.V. Chekhova, M.V. Fedorov. The Schmidt modes of biphoton qutrits: Poincare-sphere representation. *J. Phys. B: At. Mol. Opt. Phys.,* 46(095502): 1-10, 2013.
7. S. Alexander, O. Entin-Wohlman, R. Orbach. Relaxation and nonradiative decay in disordered systems. I. One-fracton emission. *Phys. Rev. B.* **32,** 10: 6447-6455, 1985.
8. V.S. Abramov. Fractal induction, avalanche, self-induced transparency, the echo in the model nanosystem. Materials of the X International Symposium on photon echo and coherent spectroscopy (PECS'2013). Yoshkar-Ola: FSBEI HPO: 78-86, 2013.
9. J. Balewski, A. Krupp, A. Gaj et. al. Coupling a single electron to a Bose-Einstein condensate. *Nature* **502,** 7473: 664-667, 2013.
10. H.-J. Stockmann. *Quantum Chaos. An Introduction.* Cambridge Univers. Press, 1999.
11. Jan Awrejcewicz, V.A. Krysko. *Chaos in Structural Mechanics*. Springer-Verlag Berlin Heidelberg, 2008.
12. C.H. Skiadas, C. Skiadas. *Chaotic Modeling and Simulation: Analysis of Chaotic Models, Attractors and Forms.* Taylor and Francis/CRC, London, 2009.
13. M.V. Zakrzhevsky, R.S. Smirnova, I.T. Schukin, et all. *Nonlinear dynamics and chaos. Bifurcation groups and rare attractors.* Riga, RTU, Publishing House, 2012.
14. O.P. Abramova, S.V Abramov. Fractal nanotraps based on quasi-two-dimensional fractal structures. *Dynamical Systems Theory* (Editors J.Awrejcewicz et. al.) DSTA 2013, Lodz, December 2-5, Poland: 71-80, 2013.
15. V.S. Abramov. Fractal dislocation as one of non-classical structural objects in the nano-dimensional systems. *Metallofiz. i Noveishie Tekhnologii*. **33,** 2: 247-251, 2011.
16. V.S. Abramov. Correlation Relations and Statistical Properties of the Deformation Field of Fractal Dislocation in a Model Nanosystem. *Chaotic Modeling and Simulation (CMSIM) Journal.* **3**: 357-365, 2013.
17. V.S. Abramov. Behavior of the deformation field of fractal dislocation in the presence of bifurcftions. *Bul. of Donetsk Nat. Univers.* **Ser. A,** 2: 23-29, 2011.
18. V.S. Abramov. Features of statistical properties of the deformation field of the fractal dislocation. *Bul. of Donetsk Nat. Univers*. **Ser. A,** 1: 105-113, 2012.
19. O.P. Abramova, S.V Abramov. Governance of Alteration of the Deformation Field of Fractal Quasi-two-dimensional Structures in Nanosystems. *Chaotic Modeling and Simulation (CMSIM) Journal*. **3**: 367-375, 2013.

20. V.S. Abramov. Inverse structural states of the stochastic deformation field of fractal dislocation. *Fizika i Tekhnika Vusokikh Davleniy*. **23**, 3: 54-62, 2013.

Chaos in Digital Currency Markets

Ergun Eray Akkaya[1], Ahmet H. Yildirim[2], Avadis S. Hacinliyan[1]

1.Yeditepe University, Kayisdagi, Istanbul, Turkey
2. Sakarya University, Adapazarı,Turkey
E-mail: eeakkaya@gmail.com

Abstract: Bitcoin was introduced in 2009 as an open source, peer-to-peer payment network for sending payments using a client software. Bitcoin has lower transaction fees compared to credit card processors which makes it a preferable transaction agency for merchants. In this paper, daily exchange prices of bitcoin in the years of 2011 to 2014 for different currencies have been analyzed using nonlinear time series analysis techniques. To apply the analysis, phase space is reconstructed by using delay time obtained from mutual information and autocorrelation of data with an embedding dimension suggested by the false nearest neighbors method. Calculated positive Lyapunov exponents indicate a possible chaotic behavior.
Keywords: Chaotic modeling, Time series analysis, Mutual information, Embedding dimension,Dynamical systems.

1. Introduction

Bitcoin's main purpose is to create a payment mode which is not controlled by any agency (by bank, government etc.). They are not printed, like dollars or euros. They are produced by lots of people running computers all around the world. Currently, twenty five new Bitcoins are released with each block every ten minutes. However, this will be halved to 12.5 BTC (Bitcoin unit) during the year 2017 and halved continuously every four years after until a hard limit of twenty one million Bitcoins is reached. An algorithm that becomes exponentially more difficult over time controls the rate of supply.
In this paper we involve time series analysis of experimental data from the average daily currency data of Bitcoin in the international software market. For now, we examine USD and Euro parity of Bitcoin in given time interval.

2. Theory and application

We must first examine the delay time in order to construct the phase space. If the time delay is taken too short then components of the reconstructed vectors will be close to each other, causing the state space picture to appear on the diagonal line, therefore we will have loss of information about the real system. On the other hand using a too long delay time will cause the correlations between the components of reconstructed vectors to be lost and signals will be mistakenly recognized as random. Information between a random variable and another random variable called mutual information. We can only observe our

7th CHAOS Conference Proceedings, 7-10 June 2014, Lisbon Portugal
C. H. Skiadas (Ed)

sending information to a channel by getting back the information coming from that channel. For example, let X and Y be random variables with common distribution p(X,Y). The joint probability of observing x by a measurement of X and observing y by a measurement of Y, $P_{xy}(x;y)$, should be different from the product of the individual probabilities of measuring x and y out of the sets X and Y respectively, P(x) and P(y) if there is correlation between the two sets. The logarithm of that ratio in bits is therefore called the average mutual information of X and Y given by $\log_2 \frac{P_{XY}(x\ ;y)}{P(x)P(y\ )}$. The weighted average of the average mutual information is given by the following Formula;

$$\mathrm{I(X;Y)} = -\sum_{x}\ \sum_{y} P_{XY}(x;y\ ) \log_2 \frac{P_{XY}(x;y)}{P(x)P(y)}$$

To apply this formula to time series analysis, we assume that S(n) is Set X and S(n+t) is Set Y. Here we obtain the average mutual information as follows:

$$\mathrm{I(t)} = -\sum_{x}\ \sum_{y} P(s(n+t),s(n)) \log_2 \left[\frac{P(s(n+t),s(n))}{P(s(n+t))P(s(n))} \right]$$

$$I(X:Y) = D(p(x,y) \| p(x)\,p(y))$$

$$I(X;Y) = \sum_{x}\sum_{y} p(x,y) \log \frac{p(x,y)}{p(x)\,p(y)}$$

Where p(x) and p(y) are the probability distributions and the entropy is the distance between actual distribution and the distribution where the mutual informations are equal. Figure 1 shows parity prices between 2011 and 2014 taken from bitcoincharts.com.

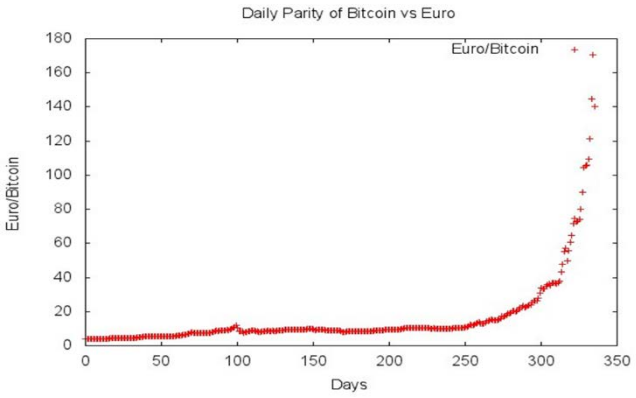

Fig. 1. Daily parity of Euro versus Bitcoin

Then by using the TISEAN programming tool package, we find the mutual information as shown in Figure 2.

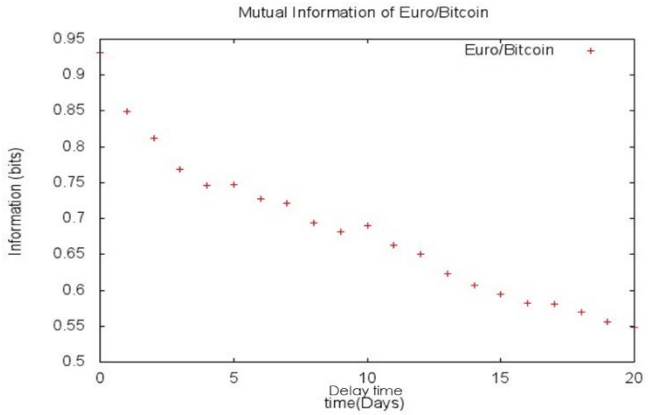

Fig. 2. Mutual information of parity Euro versus Bitcoin

To estimate the delay time we find the minimum of the mutual information which is four. The delay time is needed for finding the embedding dimension. If the embedding dimension is less than the actual dimension, points which are not neighbors on the original attractor fall into same neighborhood. Then finding false-nearest neighbors of all points on embedded attractor is necessary. We can show time delayed vector of nearest neighbors and distance in d+1 dimension of between two neighbors can be calculated like this;

$$\vec{y}_{NN}(k) = \left[S_{NN}(k), S_{NN}(k+\tau), ..., S_{NN}(k+(d-1)\tau)\right]$$

$$\left[R_{d+1}(k)\right]^2 = \left[\sum_{m=1}^{d+1}\left[S(k+(m-1)\tau) - S_{NN}(k+(m-1)\tau\right]^2\right]$$

$R_{d+1}(k)$ can be expressed in terms of $R_d(k)$ as

$(R_{d+1}(k))^2=(R_d(k))^2+(S_{NN}(k+(m)t)-S(k+(m)t))^2$.

From this result we can define a threshold value $R_T(k)$ using

$$\frac{(S_{NN}(k+(m)t) - S(k+(m)t))}{R_m(k)} \rangle R_T(k).$$

Note that we are embedding a one dimensional signal originating from a system with arbitrarily dimensionality, hence we use this criterion to find the appropriate embedding dimension in the delay vector, by looking at the point where the number of false neighbors stabilize.

Chaoticity is expressed in terms of Lyapunov exponents. To calculate this, we start with two nearby trajectories separated by a distance |x(0)|. At time t, separation is $\delta x(t)=\delta x(0)\ \exp(\mu t)$. The average of μ, the rate of exponential separation over the trajectory is the Lyapunov Exponent. In an N dimensional system, we can change δx(0) in N independent ways so that there are N Lyapunov exponents.

The Lyapunov Exponent is calculated as follows, First, find a reference point S_{n0} and let U be a hyper sphere in a distance ε.

$$S(\Delta n)=\frac{1}{N}\sum_{n0=1}^{N}\ln\left[\frac{1}{\left|U(S_{n0})\right|}\sum_{S_n\in U(S_{n0})}\left\|S_{n0+\Delta n}-S_{n+\Delta n}\right\|\right]$$

If ε is too small, we cannot find neighbors, if it is too large, a periodic component may be missed. Secondly, for different values of ε, if the graph of S(Δn) vs Δn has positive slope, we have positive Lyapunov exponent. Positive Lypaunov exponent means that there is a chaos.

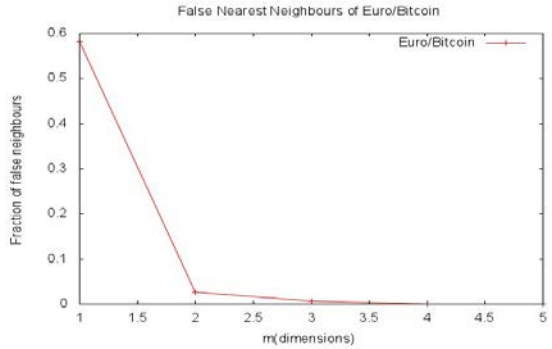

Fig. 3. False Nearest neighbors of Euro/bitcoin

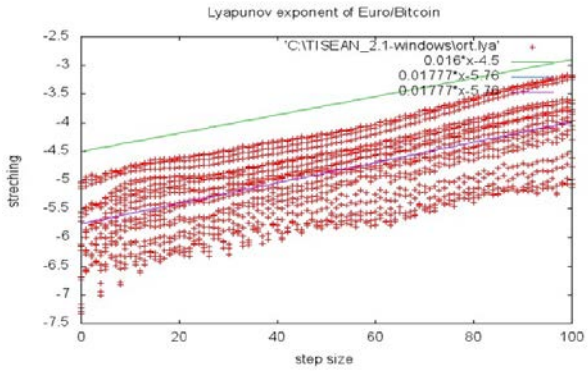

Fig. 4. Lyapunov exponent of Euro/bitcoin

As you can see in Fig. 4. Lyapunov exponent shows a positive increase therefore, we can conclude chaotic behavior. The same analysis is made for US Dollar parity and we can again see a positive Lyapunov exponent

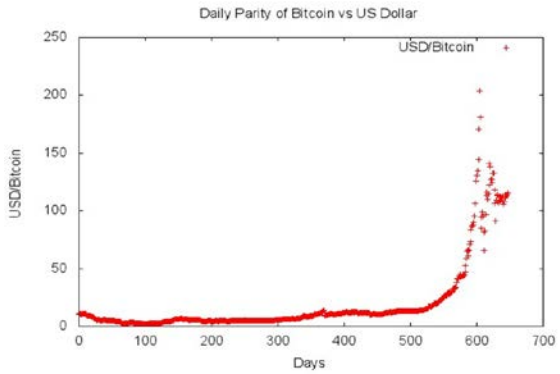

Fig. 5. Daily parity of US Dollar vs Bitcoin

In Fig. 5. Daily parity of dollar is shown and mutual information and false nearest neighbors are observed and finally positive Lyapunov exponent is observed in Fig. 6.

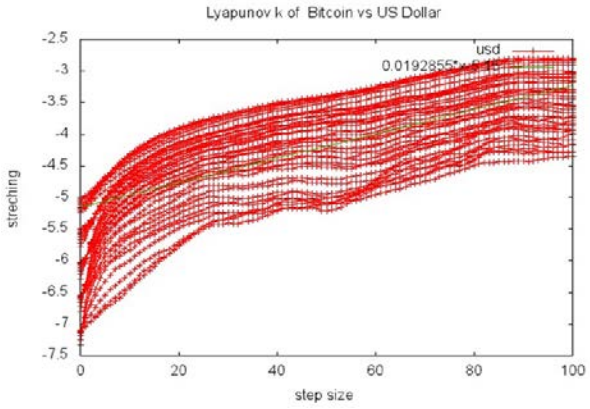

Fig. 6. Lyapunov exponent of US Dollar/Bitcoin

With the globalization and last decades, financial markets have become more sensitive and interactive. Furthermore, digital currency becomes important role for financial market because of its better purposes. In this study, the Bitcoin parity has been analyzed through chaos theory and nonlinear time series to investigate whether bitcoin also follows typical market trends these methods really determines market behavior. The results of the analyses show that methods based on chaos theory explain the financial data better than classical time series analyses methods.

3. Conclusions

Daily average currency flow data from USD and Euro parity of Bitcoin are examined. The data expands through the years nearly 2011-2014. The values obtained for delay time, embedding dimension and maximal Lyapunov exponents are shown. Calculated positive maximal Lyapunov exponent indicates a possible chaotic behavior for the Bitcoin currency dynamics. A further study can be on the dimension of the attractor will reveal more information about the chaotic behavior of the digital currency.

References

1. James Fox. Bitcoin and Digital currency: The new World of Money and Freedom, Laissez Faire Books.
2. Kathleen T. Alligood, Tim D. Sauer, James A. Yorke. Chaos: An Introduction to Dynamical Systems. Springer Books
3. http://www.bitcoincharts.com.
4. http://www.mpipks-dresden.mpg.de/~tisean/
5. O. Özgür Aybar "Possible Chaoticity in Condensed Matter System", M.Sc. Thesis (Prof. Dr. Y. Skarlatos –Prof.Dr.Avadis Hacınlıyan), Boğaziçi University, Istanbul (2008)
6. H. A. Yıldırım, Ph.D. Thesis (Prof. Dr. Y. Skarlatos –Prof.Dr.Avadis Hacınlıyan) "Chaotic Structures in Conductivity Mechanisms" Boğaziçi University, Istanbul (2005)
7. A. S. Hacınlıyan, O. O. Aybar, İ. Kuşbeyzi Aybar, M. Kulalı, Ş. Karaduman "Signals of Chaotic Behavior in Middle Eastern Stock Exchanges", Chaos and Complex Systems–Proceedings of the 4th International Interdisciplinary Chaos Symposium, Springer, ISBN 978-3-642-33913-4, pp. 353-356, (2013).

2-Phase model for population growth

Vladimir G. Zhulego[1] , Artem A. Balyakin[2],

[1] Department of analysis and forecast, NRC "Kurchatov Institute", Moscow, Russia, (E-mail: zhulego@mail.ru)

[2] Department of scientific and technical programs and projects, NRC "Kurchatov Institute", Moscow, Russia, (E-mail: Balyakin_AA@nrcki.ru)

Abstract.
We discuss the 2-component model of population growth when different types of dynamics are attributed to rural and urban population respectively. We suppose the birth rate to be higher for rural areas, and death rate to dominate for cities. The flow between areas compensates these effects. This approach can reduce the number of parameters usually used for population growth behavior. We also discuss the socio-economic aspects of the model: the ability to control population size by adjusting the flow of people from the city to the countryside, and the trends in the urban and rural population. Finally the Earth population model is proposed.

Keywords: population growth, chaotic simulation, modeling of socio-economic processes.

1. Introduction

The problem of numerical simulation of population dynamics attracts a lot of attention in both natural and social sciences. Particularly this issue was supposed to be of great importance when it was proved that the population growth rates were increasing, and the simplest modeling of such dynamics inevitably leads to overpopulation of the planet (eg, a Malthusian crisis). Furthermore, a precise date of overpopulation was esteemed as 2004.

Thus, the "overpopulation problem" initiated a thorough statistical study of the dynamics of population growth, as well as many theoretical works arose, clarifying model representation of such dynamics. Along with Malthus classic work, it should be mentioned Verhulst model [1], Kapitsa model [2], Forrester world-system model [3] and many others. As it turned out, the rate of population growth crucially determines the growth rate of GDP, and this fact has largely spurred interest in the subject [4,5].

7th CHAOS Conference Proceedings, 7-10 June 2014, Lisbon Portugal
C. H. Skiadas (Ed)

The most interesting dynamics is connected with so called "demographic transition point" when population growth sharply decreases and number of people achieves stable value. At the same time, all proposed model are unlikely to describe the entire dynamics of the population: the explosive growth of the initial time, saturation stage (demographic transition point) and then subsequent stabilization of the population. Statistical data are used to adjust the model, and often numerical simulation is reduced to finding appropriate coefficients that would fit the observed results (see, e.g. [6]).

We argue that much more productive approach may be based on physical arguments; in particular, we believe that the population should be considered as two-phase system – "rural population" and "urban population", with each phase to behave under its own laws of growth, having, however, a flow between two phases. This view of the population dynamics growth can decrease the number of arbitrary parameters in the model, and also give additional arguments and levers to control the pace of population growth that is important for countries experiencing problems with overcrowding and/or depopulation challenges. In addition, it becomes possible to construct a universal model describing population dynamics on the Earth.

In this paper we propose and discuss the 2-component model of population growth when different types of dynamics are attributed to rural and urban population respectively. We exclude from consideration the initial stage of human civilization, when the population was too small to introduce residents' differentiation, and not consider the case of population stabilization.

We assume that the entire population can be divided into two relatively independent groups (phases), focused respectively on the intensive and extensive ways of development - urban and rural areas. Note that these concepts are not geographical, and probably reflect the attitude of the population to the production of wealth and investing in future generations and lifestyles. The most important characteristic that allows extracting these two groups, apparently, is the population density per square kilometer. The problem to calculate/evaluate this value would be another interesting task that we will not consider in our work.

2. Statement of the problem

We suppose there is a closed area (no emigration) with an unlimited resources supply (i.e., country). Let us denote urban population as x, the rural population as y, and the time variable as t.
Then, in the general case, we can write

$$\begin{aligned} \frac{dx}{dt} &= f(x, y, \lambda) + w(x, y, \lambda) \\ \frac{dy}{dt} &= g(x, y, \lambda) - w(x, y, \lambda) \end{aligned} \tag{1}$$

Here λ is the institutional parameter responsible for the particular worldview of people and their relationship to birth, death, change of residence, and taking into account both objective (laws and restrictions) and subjective (the desire to

move to the big city, or, conversely, the nature) factors. The functions describing the change of the urban population and the rural population are *f* and *g* respectively. The function of the population flow from one community to another is *w*. We stress that function *w* is greatly influenced by authorities, and can differ from country to country. Note that time is not explicitly included in the functional relationship. Our task is to study the possibility of governing the dynamics of the system changing function w (i.e., changes in public policy).

Using qualitative considerations (based on common approach to describe the dynamics of living organisms like predator-prey system, the game "Life", etc.) we can conclude that for a fixed urban population *x* function *w(y)* is strictly increasing function without saturation (i.e. is convex and the derivative does not change its sign). The qualitative form of the function w(y) is shown in Figure 1a. Similarly, in the case of constant values of rural population y we construct qualitative form of the function w (x), the population flow increases linearly for small values of x and subsequently begins to decrease due to resource constraints and increasing population density in the city (Fig. 1b).

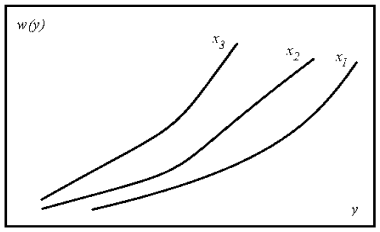

Typical behavior of w(y), $x_3 > x_2 > x_1$.

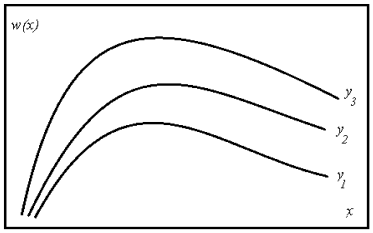

Typical behavior of w(x), $y_3 > y_2 > y_1$ ..

Fig. 1. The behavior of the function *w*.

Based on the qualitative analysis of the figures 1a,b we propose the following form of the function *w*, satisfying all the properties listed above:

$$w(x, y, \lambda) = \beta \frac{xy}{x^2 + \alpha^2} \qquad (2)$$

Here the numerator *xy* is proportional to the number of meetings between urban and rural residents, that can be treated as a "reassurance" of a resident to change his/her address with probability β. The denominator in the formula (2) imposes restrictions on the movement of villagers into the town with a large urban population. In extreme cases, when the frequency of meetings has no effect on the decision of the villagers move to the city, all of them with some degree of probability take the decision to move. However inures limiting factor associated with the limited space and high population density in urban areas, which is directly proportional to x^2. Term α^2 is introduced to eliminate peculiarity at $x=0$, and reflects the minimum number of people needed the population becomes “city”. Estimates of population dynamics (parameter fitting

formula for hyperbolic growth) give us the number of 60-70 thousand people (the size of the human community, when main role play statistical factors rather than personal ones).

For the sake of convenience, we will assume the function *w* always positive, but in general negative function is also possible, and it would represent the flow in reverse (from city to the countryside).

Thus, the proposed model reduces the institutional parameter λ to two parameters α and β. Note that we do not consider the simplest case when *w=const.*

Let us choose the functions *f* and *g* in the simplest form:

$$f = -ax \ , \ g = by - cy^2 \tag{3}$$

The meaning of this choice is that the urban population decreases, while the rural population is growing, but there is a limit due to the finite resources. In practice, the choice of functions (3) permits us to formulate one of the differences between urban and rural areas: the countryside is a source of replenishment of the population, it possesses a positive population growth, and the city is characterized by a decline in population, as it is more inclined in the production and creation tools/services, both for city's sake and for the village.

Thus, the proposed two-component (two-phase) model can be rewritten in a following form:

$$\begin{aligned} \frac{dx}{dt} &= -ax + \beta \frac{xy}{x^2 + \alpha^2} \\ \frac{dy}{dt} &= by - cy^2 - \beta \frac{xy}{x^2 + \alpha^2} \end{aligned} \tag{4}$$

These equations however, do not exhibit complex behavior, and only have stable points solutions; the model initially contains no "points of demographic transition" or "overpopulation problem". This is close to the reality, but needs some improvement: we assumed that the response of the system is instantaneous for variables *x* and *y*. To account for the effects associated with the maturation of people, and make the complex dynamics possible, we take into account the presence of delay in the system. Namely, we rewrite system (4) as a

$$\begin{aligned} \frac{dx}{dt} &= -ax(t) + \beta \frac{x(t-\tau)y(t-\tau)}{x^2(t) + \alpha^2} \\ \frac{dy}{dt} &= by(t) - cy^2(t) - \beta \frac{x(t-\tau)y(t-\tau)}{x^2(t) + \alpha^2} \end{aligned} \tag{5}$$

The meaning of the last term in this case is that the move from rural to urban areas is carried out by adults, usually without family. Accordingly, the decision shall be taken in the "meetings" with the same people over the age of the city (almost, it comes to comparing features/lifestyles in the countryside and in the city for people of the same age group). At the same time limiting factor (the denominator in the last term) still depends on the current urban population.

Also to reduce the number of control parameters we use following renormalization.

$$t' = t/\tau,\ x' = x/\alpha,\ y' = y$$

And introducing the notations:

$$A = a\tau,\ B = b\tau,\ C = c\tau,\ D = \beta\tau/\alpha^2$$

Then, omitting the primes in the new variables, we obtain the system:

$$\begin{aligned} \frac{dx}{dt} &= -Ax(t) + D\frac{x(t-1)y(t-1)}{x^2(t)+1} \\ \frac{dy}{dt} &= By(t) - Cy^2(t) - D\frac{x(t-1)y(t-1)}{x^2(t)+1} \end{aligned} \tag{6}$$

System of equations (6) will be the final mathematical formulation of the proposed model.

From the physical meaning of the system, all variables must be positive (on the parameters *A, B, C, D* this requirement was imposed initially). Lag time now is always 1. In numerical simulation we expect that the most typical regime still to be stationary mode or with mild oscillations near the equilibrium point (the latter is quite typical of early human societies lived slash agriculture, where the population is growing at the beginning, and then, because of the impoverishment of resources began to decrease).

This model contains now modes of complex dynamics, they are possible in this system due to the presence of external feedback. Oscillatory or "chaotic" modes in this system are associated with huge costs (depopulation in towns or villages, the collapse of infrastructure, etc.) In practice, if a management decision could transfer the system from stable stationary mode to complex dynamics, it would mean that the proposed action is a mistake.

Let us estimate the numerical values of the parameters in the system (6). The parameters A, B, C are responsible for the share increase (decrease) of the population in a time where, in comparison with available statistics, we find that they all vary from zero to one. Greatest arbitrariness is related to the choice of the parameter D, because it depends on a set of institutional factors such as persuasion factor β or α .

3 The stability points analysis

Let us analyze the system (6) for stability. There are always two trivial solutions: x=y=0, and x=0, $y = B/C$. The first solution corresponds to the lack of human civilization or the initial point, and second corresponds to collapse of urban civilization. For the classification of other solutions we obtain the following equation for fixed points (recall that within the framework of our model x> 0):

$$y = \frac{A}{D}\left(x^2+1\right), \qquad CAx^4 + (2CA - BD)x^2 + D^2x + CA - BD = 0 \tag{7}$$

To find the exact analytically solution in this case is impossible, however, we can give the following estimates. If CA-BD> 0, the solutions of

(7) does not exist. If CA-BD <0, but 2CA-BD> 0, then there is one solution, but if 2CA-BD <0, it is possible one or the two solutions. Type the appropriate parameter plane shown in the figure below. We note that there are 3 areas that can perform different dynamics. For the first area with 2 stationary points one of them is always unstable, thus resulting regime is expected to be constant. In the second area 2 different stable solutions are possible. And in the last area complex dynamic and interchange between different stable stationary points are possible.

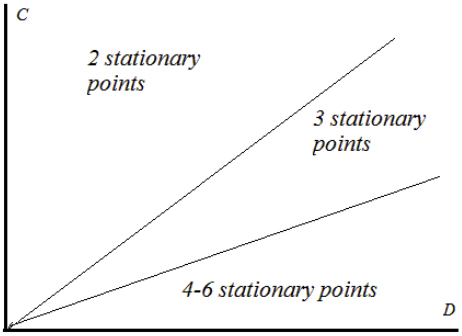

Fig. 2. Parameter plane for stationary points at Ox-axis. Stability analysis.

4. Numerical simulation

Further we will discuss the results of numerical simulations conducted by the Runge-Kutta of 4th order. Time step is $dt = 0.01$, and the parameters values are given in figure captions. Note that at this stage we do not set the task to find the exact quantitative relationship between real data and parameters used for computer modeling, we are focusing on the opportunity to effectively control the dynamics, to change between regimes, etc. In numerical simulations we proceed as follows: for the time 1 (dimensionless time delay) we numerically solve the system (6) without delay, and starting at time 1, we consider the term with delay. Thus we can avoid the need to set the initial conditions in the interval (0, 1).

Below we represent the parameter plane for fixed values of *A*, *B* with varying *D*. We note a good agreement with theoretical calculations (compare fig. 2 and 3). In the lower region, where the number of fixed points is large, it is possible to realize the complex dynamics. Thus, we mark the area of chaotic oscillations with red, and periodic oscillations with different period with green. Unstable (nonphysical) behavior is also present. We note that the region of periodic oscillations is adjacent to the area of chaotic behavior, hence the periodic oscillations in the system can be regarded as precursors of the onset of chaos and/or unstable solutions. The last ones due to the nature of studied system should be avoided in reality.

We also plotted 3 regions with stable solutions: the first one with 2 stationary points is characterized by the situation when after transient proves x=0, and y=const. It is pure rural community, when all population is

concentrated in countryside, AC>BD that means death and restriction of the rural population growth (parameter C) play more important role than birth rate and population flow. People are more likely to die than to survive, and the rest of population settles in rural areas. In the second area stable solution is represented with stable rural and urban population, but rural people dominate. This situation can be regarded as traditional society when cities are rare and most of population prefer to live in countryside. However with the increase of D and/or decrease of C (the flow grows and/or limitations for rural population become weaker) the stable solution for urban population begins to overcome the rural one. It could occur either because of the cities to become more "popular" (parameter D), or when rural area cannot support more number of people (decrease of C). Both tendencies make people to go away from the countryside. Also near abscissa (low C) there is a narrow area of stable solution when x=0, y=const. It happens when because of the decrease of C the number of people that can survive in rural area becomes too small to be enough for both phases. People thus have to choose where to live, and they prefer to stay where they are born rather than to move away.

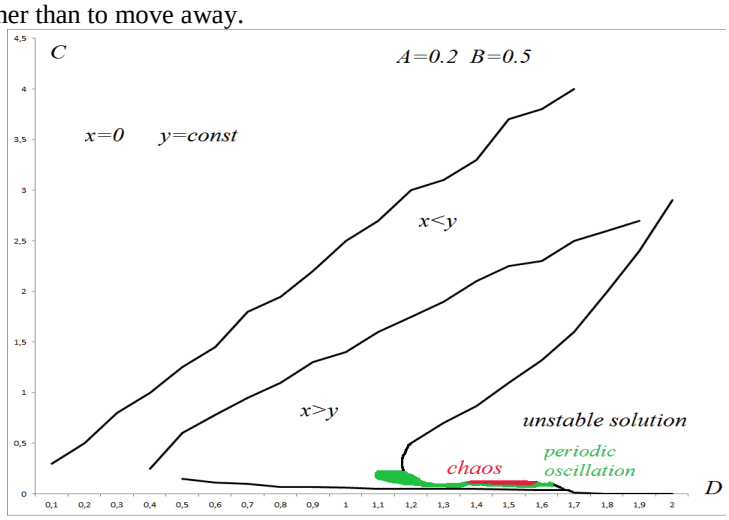

Fig. 3. Parameter region at A = 0.2. B = 0.5

Typical time series are presented in fig. 4-9. Urban population is represented by red, rural – by green, and total number of people – by black solid line. Initial conditions were chosen x=0,1, y=0,9.

Usually after short transient process a stable solution is observed. 2 typical situation are presented in fig. 4 and 5. In the first case there are both rural and urban people, in the second case cities disappear.

Oscillations though being rather rare can also be observed. They are more likely to damp with very long transient process (fig. 7), but also can be stable (fig. 6). This dynamics can be attributed to Neolithic societies when people use the land as much as they could and having depleted it they started to starve and consequently die. However it is not typical for nowadays

communities, and thus should be avoided. Complex and even chaotic behavior can also be found, but we present it here as an example of non-physical dynamics, since in usual life this would be the signal of wrong managerial solutions. We should note that area of complex dynamics is very small, and that can also be treated as model adequacy.

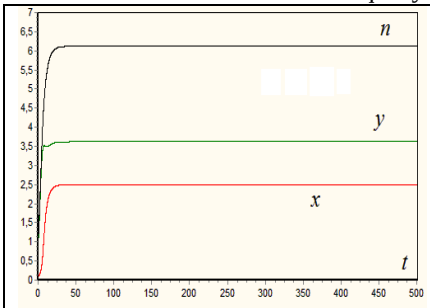

Fig. 4. A=0.2; B=0.5; C=0.1; D=0.4 Transition to stationary mode where rural population exceeds the urban

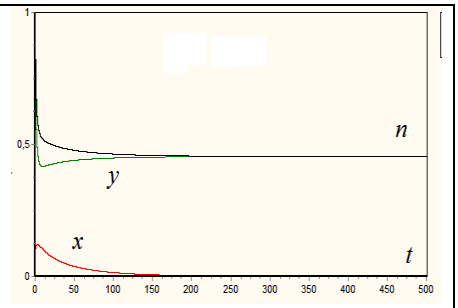

Fig. 5. A=0.2; B=0.5; C=1.1; D=0.4; Transition to stationary mode, when the urban population disappears.

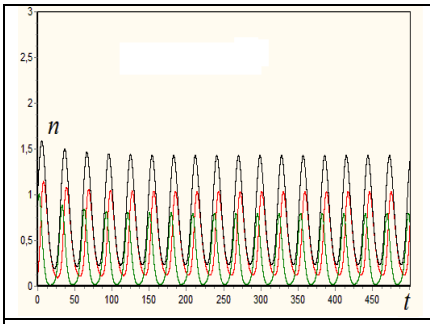

Fig. 6. A=0.2; B=0.5; C=0.3; D=1.1 Periodic oscillations

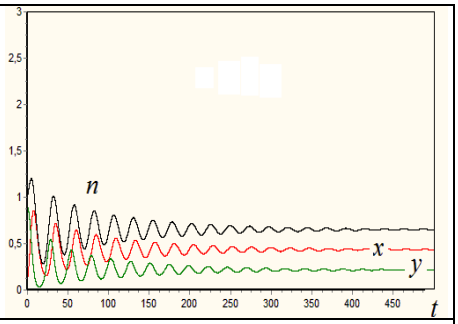

Fig. 7. A=0.2; B=0.5; C=0.45; D=1.1; Damped oscillations.

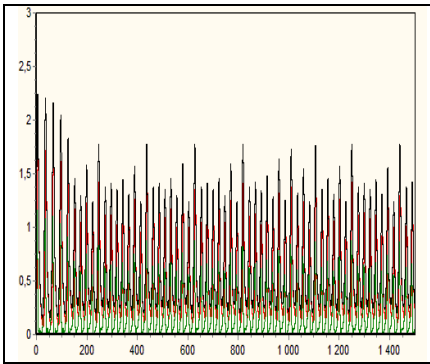

Fig. 8. A=0.2; B=0.5; C=0.1; D=1.6; Chaotic oscillations

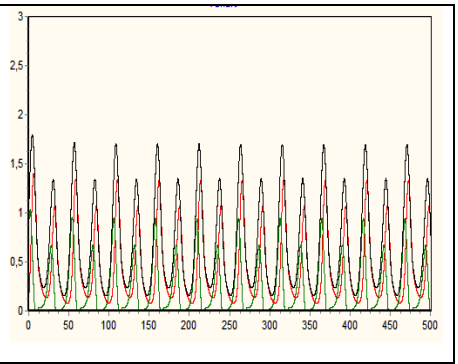

Fig. 9. A=0.2; B=0.5; C=0.19; D=1.5; Multi periodic oscillations (2-period)

5 The problem of controlling the system dynamics

The most serious problems associated with population growth faced by governments is a overpopulation problem and demographic crisis or extinction of the population. In this connection let us consider how to manage the system dynamics. Suppose the government implements measures that can be reflected as a change in the values of the system parameters *A, B, C, D* and/or the sudden change in the number of *x, y* (artificially people moved from the countryside to the city, or vice versa). Clearly, the parameters *A, B, C* can not be changed dramatically; they are responsible for the traditional approach to family formation (*B, C*) or reflect the outcome of long-term policy in the field of medicine (*A*). Their variations are insignificant and they are extended in time. For these reason we will call this group of parameters as adiabatic.

On the other hand, the parameter *D* can be changed quite drastically: for example, the frequency of "meetings" can be increased or decreased by creating artificial barriers to entry the city or leave the village (strict registration rules), or one can modify α providing residents of the city more "rustic" conditions related to population density (buildings as the private sector). Parameter *D* also could include a variety of unrealistic events (meteor fall, epidemics, etc.).

In the numerical simulation we will implement all the parameter changes at time $t = T/2$. Some results are presented below.

First, we consider additional flow added to the natural one. We studied both constant summand, and summand proportional to rural population. System dynamics does not change, and new system can be reduced to the old one by re-normalization (fig. 10). Then we study the case when there is a 10% shift of the population (people are forced to move from countryside to the cities. The similar situation occurred in collectivization in Russia or during fencing in England). Since mostly solution are stable this momentary shift does not influence system dynamics, and after rather short transient process system returns to its initial state (fig. 11). In both case the system damps the abrupt changes, thus we conclude that such hard measures cannot give expected results.

Quite fast "curb overpopulation" can be achieved by cross-flow of the rural population in the urban population in a city where the birth rate is significantly reduced. Suppose, for example, at some point in mortality fell, reaching 96% of the original level. In this case, there would be an increase in urban population, but at the same time the rural population would slightly decrease, too (that happens because of the limiting factor inversely proportional to the square of the urban population). Total number of people, however, increases. This mode is shown on Fig.12. Similar behavior can be observed and if the birth rate in villages increased by 4% (fig. 13). In that case rural population grows and thus increases the number of citizens. Qualitatively similar behavior can be seen if we increase death rate in cities of decrease birth rate in countryside: both population in rural and urban areas decreases, and total number of people diminishes. It is interesting to note that the change in life conditions in villages influences the system dynamics (and the total number of

people) more than similar changes in urban life (we plotted the time series for the change of 4% in comparison to the initial values – both in decrease/increase).

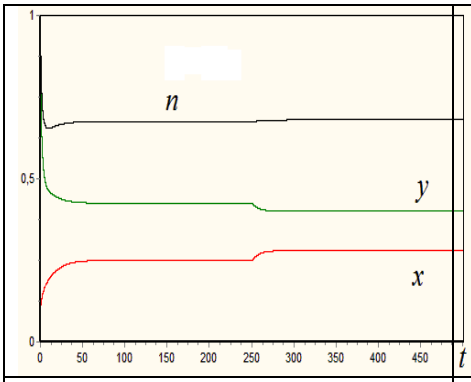

Fig. 10. A=0.2; B=0.5; C=0.9; D=0.5; Shift is 0.1 in dimensionless variables when to the "natural" overflow adds an additional inflow of artificially created

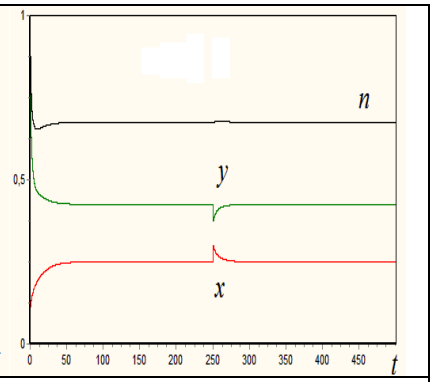

Fig. 11. A=0.2; B=0.5; C=0.9; D=0.5; Shift is 0.1 in dimensionless variables. Sharp one-time change in the number of cities and villages population

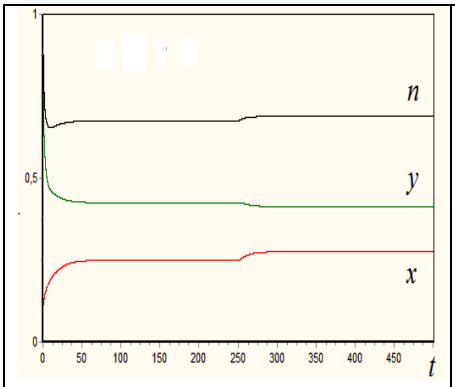

Fig. 12. A=0.2; B=0.5; C=0.9; D=0.5; Mortality in city fell, reaching 96% of the original (parameter *A*)

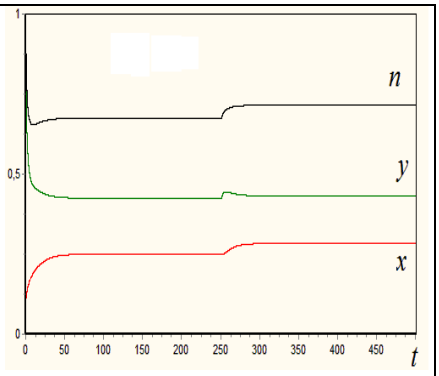

Fig. 13. A=0.2; B=0.5; C=0.9; D=0.5; Birth rate in the countryside is growing at 4% (parameter *B*)

The obtained results may, in particular, explain why the increase in life expectancy in urban areas (ie, a mortality decrease) does not lead to such dramatic changes as a decline in fertility in the village. We stress that the situation in the countryside (source of population) is decisive. At the same time, our results show that the policy can be directed only one of the population groups to achieve the result and do not necessarily affect both the city and the countryside, moreover, it may be advantageous to use that institutional arrangements to only one part of the population.

We also studied the case when the parameters *A, B, C* remain unchanged, but at time t/2 parameter D varies. As it turned out, the system is very sensitive to changes in this parameter. Especially one can achieve periodic oscillations from stationary ones, or even chaotic. Some examples are presented in fig. 14.

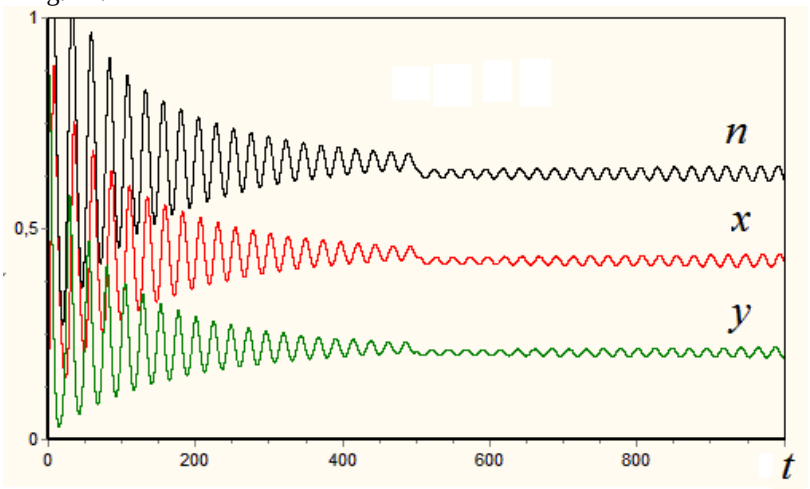

Fig. 14. A=0.2; B=0.5; C=0.43; D=1.1; An example when the parameter D varies by only 4%, but damped oscillations become stable.

The changes in institutional parameters can be implemented easier, and can be performed in a short period of time. However adiabatic parameters evolve over time, allowing the system to adapt to the new situation. They are thus highly rigid. Obviously, the best way to influence the dynamics of the system lies in the combination of exposure to adiabatic and institutional parameters.

6 Two-component model of population growth of the Earth

On a base of the foregoing observations, it is possible to formulate a model of population growth of the Earth in the form of a chain of equations describing each country separately. Obviously, just scaling the resulting model is not possible, since the processes of flow of the population in different countries has quite different nature. In addition we have the processes of migration between countries. Apart from introducing such a model term describing the flow of rural population in the city, we must also take into account immigration, i.e. overflow of the population of one country to another. For some countries, this flow is the main source of population growth (e.g. the U.S.). This term is logical to take in a similar term describing the flow of rural population in the city as in a single country.

We assume the process of emigration occurs regularly, and go into exile in the first place for economic reasons: travel for higher wages, better living conditions, the medicine. And emigration has its source mainly in urban

residents who know foreign languages, and have better opportunity to travel. Besides these processes emigration can occur because of war, natural disasters and other force majeure, but they will not be taken into account at this stage.
Given all this system of equations will have the following form:

$$\begin{aligned}\frac{dx_i}{dt} &= -a_i x_i(t) + \beta_i \frac{x_i(t-\tau_i)y_i(t-\tau_i)}{x_i^2(t)+\alpha_i^2} + \sum_k \gamma_{ik} \frac{x_i(t-\tau_i)x_k(t-\tau_k)}{x^2{}_i(t)+x^2{}_k(t)+\alpha^2{}_i+\alpha^2{}_k} \\ \frac{dy_i}{dt} &= b_i y_i(t) - c_i y_{i_i}{}^2(t) - \beta_i \frac{x_i(t-\tau_i)y_i(t-\tau_i)}{x_i^2(t)+\alpha_i^2}\end{aligned} \quad (8)$$

Here i = 1,2,3, ... N denotes the total number of countries in the world. Totally turns out 2N differential equations. The Earth's population will be calculated as a simple sum of all ($x_i + y_i$). Analysis of the system (8) can be carried out numerically, similar to the analysis of the system (6). Detailed analysis of this system will be presented in further publications.

Conclusions

The discussed approach to study population dynamics allows introducing less numbers of variables to describe population growth. It also can explain some peculiarities in population dynamics and can be used for more effective managerial solutions in social aspects of human life.

Acknowledgements

This work was supported by RFBR grants 13-06-00842, and partially by 13-02-12111.

References

1. Verhulst P.F. Notice sur la loi que la population poursuit dans son accroisment. Correspondence mathematique et physique. 1838. N 10, P. 113-121.
2. Kapitsa S.P. Global population blow-up and after. The demographic revolution and information society. Moscow, 2006.
3. Forrester J.W. World Dynamics. Wright-Allen Press. 1971.
4. Solow R.M. (1956). A Contribution to the Theory of Economic Growth. Quarterly Journal of Economics 70 (1): 65–94.
5. Akaev A, Sadovnichy V and Korotayev A. On the dynamics of the world demographic transition and financial-economic crises forecasts. Eur. Phys. J. Special Topics 205, 355-373 (2012).
6. Turchin P. Complex Population Dynamics: a Theoretical/Empirical Synthesis. Princeton, NJ: Princeton University Press. 2003.

Variation of Resistancec of DNA versus the Temprature

S.Behnia[1*], S.Fathizadeh[2]

[1,2] Urmia University of Technology, Orumieh, Iran
E-mail: [1] s.behnia@sci.uut.ac.ir , [2] s.fathizadeh@sci.uut.ac.ir

Abstract: In recent years DNA has attracted much attention for its potential application in molecular electronics and nanotechnology. Numerous mechanisms have been carried out for studying the charge transport in DNA. Among which a polaron hopping mechanism has turned out to be a prospective candidate for modeling the coupling between electronic and lattice configuration. In this regard, Su-Schrieffer-Heeger (SSH) model describes the coupled structural and electronics aspects of DNA. In this work Mean Lyapunov exponent (MLE) theory is proposed to study the charge transfer mechanism in DNA through SSH model. The spatial pattern of the system is disordered when MLE is large and ordered when it is small. Also, Landauer resistance is related to Lyapunov exponent via the transmission coefficient of the system. The obtained results based on the MLE theory express the effect of the temperature and external field on charge transfer and the resistance of DNA. Also it yields the best range for the field parameters.

Keywords: Charge transfer in DNA, Landaure resistance, Chaos theory, Mean Lyapunov exponent.

1. Introduction

Investigations of DNA conducting properties are very important for both classical radiobiology and quite a new science of nanobioelectronics [1]. There is clear evidence that charge injection and migration in DNA is associated with damage, mutation and repair of DNA [2]. In nanotechnology, DNA junctions have the potential of application in DNA-based drug delivery [3]. By studying the aspects of DNA single molecule conductance, it is inferred that DNA is suitable for the design of functional nanostructures in nanoelectronical devices, nanosensors, nanocercuits as well as in electrical DNA sequencing [4]. For different conditions the experimental data observed by different groups are often contradictory. Then, the argument whether DNA is a conductor [5], a semiconductor [6] or an insulator [7] and even superconductor [8] is still ambiguous. Therefore applying the physical rules in determining the charge transfer phenomena in DNA is challenging issue. May be considering the chaos

7th CHAOS Conference Proceedings, 7-10 June 2014, Lisbon Portugal
C. H. Skiadas (Ed)

theory tools could open the new horizon in understanding the problem of charge transfer in DNA. Numerous theoretical mechanisms have been carried out for studying the charge transport in DNA. Among which a polaron hopping mechanism has turned out to be a prospective candidate for modeling the coupling between electronic and lattice configuration. The tight-binding Peyrard–Bishop–Holstein (PBH) [9,10] and Su–Schrieffer–Heeger (SSH) [11,12] are two effective models, which are all based on a polaron. In the two models, overlapping Π orbitals of the DNA base pairs are thought to provide a channel for migration of charge in it. In the current study, we have used SSH model to describe the coupled structural and electronics aspects of DNA. Also, it is important to understand how the electron transport in DNA is affected by the environmental phonons. In this model, a tight-binding nanoscale linear chain is used, which is weakly coupled to the vibrational phonon modes from the environment (reservoir) via electron– phonon (e–ph) interaction. The model, characterizes the atomic displacements as classic oscillators and charge transfer phenomena with nearest neighbor tight-binding model.

Most of the introduced Hamiltonians in DNA charge transfer and the corresponding equations of motion are extremely nonlinear and have a high sensitive behavior to chosen coefficients. Also, analysis of bioinformatics data, such as the sequences derived from the structure of DNA molecules, reveals that these data are “chaotic” in the sense that along a molecule the spatial variation is analogous to the temporal variation in chaotic systems. The Lyapunov exponent is one of the most popular concepts of the nonlinear dynamics to measure how stable the systems are. In 1999 Hiroshi Shibata introduced mean Lyapunov exponent (*MLE*) in order to characterize the chaos in systems described by partial differential equations [13, 14]. The *MLE* theory has attracted researcher’s attention and has been successfully applied in several fields [15, 16]. In this work, MLE theory is proposed to study the charge transfer mechanism in DNA through the SSH model. Also, Landaure resistance is related to Lyapunov exponent via the transmission coefficient of the system. By considering the behavior of MLE, we have studied the variation of resistance of DNA in the

framework of SSH model with external phonon coupling. In the other hand, applying the electrical field, the effect of the amplitude and frequency of the field on charge transfer and resistance of DNA is studied so the best range for field parameters is selected.

2. The Model and Simulations

The studied system is consisting of the DNA lattice and an environmental optical phonon source. The Hamiltonian of the system can be modeled as

$$H = H_{SSH} + H_{Ph} + H_{e-Ph} \tag{1}$$

The first term, so-called SSH model [11, 12], has been used to simulate charge transfer in DNA with strongly internal e–ph interaction represented in classical scheme

$$H_{SSH} = \sum_n \frac{1}{2} m\dot{x}_n^2 - \sum_n [t_0 - \alpha(x_{n+1} - x_n)][c_{n+1}^+ c_n + c_n^+ c_{n+1}] + \varepsilon_0 \sum_n c_n^+ c_n + \frac{k_s}{2} \sum_n (x_{n+1} - x_n)^2 \tag{2}$$

where m is the mass of base pairs, t_0 is the hopping integral, the energy ε_0 is the orbital energy level of the molecule, x_n is the atomic displacement for the nth molecule, c_n and c_n^+ are creation and annihilation operators of an electron at the site n and α is the internal e–ph coupling constant. The last term in Eq. (2) represents the spring potential with an effective spring constant k_s.

Two last terms in Hamiltonian represent the vibrational mode at frequency ω_0 coming from the external sources and the local external e–ph interaction term, respectively.

$$H_{Ph} + H_{e-Ph} = \omega_0 \sum_n b_n^+ b_n + \gamma_0 \sum_n c_n^+ c_n (b_n^+ + b_n) \tag{3}$$

where b_n and b_n^+ are creation and annihilation operators of an phonon at the site n and γ_0 is the external e–ph coupling constant.

In the current study, we propose the effect of electrical field on charge transfer in DNA. In this regard, an AC field is applying so it provides an extra degree of freedom (frequency of field) in studying the effect of field. The corresponding Hamiltonian has the following form

$$H_{field} = -eE_0 \cos(\omega t)\sum_n nac_n^+ c_n \tag{4}$$

where E_0 and ω are the amplitude and the frequency of the field, respectively and $a = 3.4A^\circ$ is the distance between the base pairs in lattice.

The corresponding equations of motion have the following forms:

$$m\ddot{x}_n = k_s(x_{n+1} + x_{n-1} - 2x_n) - \alpha(c_n^+ c_{n-1} + c_{n-1}^+ c_n - c_{n+1}^+ c_n - c_n^+ c_{n+1}) + \xi_n(t)$$

$$\dot{c}_n = -\frac{i}{\hbar}\{\gamma_0 c_n(b_n^+ + b_n) - [t_0 - \alpha(x_{n+1} - x_n)]c_{n+1} - [t_0 - \alpha(x_n - x_{n-1})]c_{n-1}$$

$$- neaE_0 \cos(\omega t)c_n\}$$

$$\dot{b}_n = -\frac{i}{\hbar}(\omega_0 b_n + \gamma_0 c_n^+ c_n) \tag{5}$$

where $\xi_n(t)$ accounts for thermal noise, $\langle \xi_n(t) \rangle = 0$, $\langle \xi_n(t)\xi_k(t') \rangle = 2m\gamma k_B T\delta_{nk}\delta(t-t')$, with T as the bath temperature.

Stability analysis

The Lyapunov exponent is defined as the average rate of divergence of two initially nearby trajectories. It has been calculated for a single starting point. If we compute the Lyapunov exponent for a sample of starting points and then average those results, we define the mean Lyapunov exponent (MLE) for the system [17]. Then MLE will be a true indicator of the chaotic or nonchaotic behavior of the system. It expresses the disorderness of the spatiotemporal patterns of nonlinear systems. In order to investigate the characteristics of Lyapunov exponents, we have used the Jacobi matrix. Jacobi matrix, gives the linear stability of the system and the disorderness of the field variables of the system. The eigenvalues of matrix give the Lyapunov exponents [13, 14]. To

analyze the equations, it is convenient to transform the second order differential equations into an autonomous system of first order differential equation and use the finite difference method. Then we have

$$x_n^{i+1} = x_n^i + \Delta t u_n^i$$

$$u_n^{i+1} = u_n^i + \Delta t\{\frac{k_s}{m}(x_{n+1}^i + x_{n-1}^i - 2x_n^i) - \frac{\alpha}{m}(c_n^{i+} c_{n-1}^i + c_{n-1}^{i+} c_n^i - c_{n+1}^{i+} c_n^{i+} - c_n^{i+} c_{n+1}^i) + \xi_n(t)\}$$

$$c_n^{i+1} = c_n^i - \Delta t \frac{i}{\hbar}\{\gamma_0 c_n^i (b_n^{i+} + b_n^i) - [t_0 - \alpha(x_{n+1}^i - x_n^i)]c_{n+1}^i - [t_0 - \alpha(x_n^i - x_{n-1}^i)]c_{n-1}^i - neaE_0 \cos(\omega t) c_n^i\}$$

$$b_n^{i+1} = b_n^i - \Delta t \frac{i}{\hbar}(\omega_0 b_n^i + \gamma_0 c_n^{i+} c_n^{i+}) \tag{6}$$

Then we consider the $4N \times 4N$ Jacobian matrix written as:

$$B_{k,N} = \begin{bmatrix} \frac{\partial y_1^{k+1}}{\partial y_1^k} & \cdots & \frac{\partial y_1^{k+1}}{\partial y_N^k} & \frac{\partial y_1^{k+1}}{\partial u_1^k} & \cdots & \frac{\partial y_1^{k+1}}{\partial u_N^k} & \frac{\partial y_1^{k+1}}{\partial c_1^k} & \cdots & \frac{\partial y_1^{k+1}}{\partial c_N^k} & \frac{\partial y_1^{k+1}}{\partial b_1^k} & \cdots & \frac{\partial y_1^{k+1}}{\partial b_N^k} \\ \vdots & \cdots & \vdots & \vdots & \cdots & \vdots & \vdots & \cdots & \vdots & \vdots & \cdots & \vdots \\ \frac{\partial y_N^{k+1}}{\partial y_1^k} & \cdots & \frac{\partial y_N^{k+1}}{\partial y_N^k} & \frac{\partial y_N^{k+1}}{\partial u_1^k} & \cdots & \frac{\partial y_N^{k+1}}{\partial u_N^k} & \frac{\partial y_N^{k+1}}{\partial c_1^k} & \cdots & \frac{\partial y_N^{k+1}}{\partial c_N^k} & \frac{\partial y_N^{k+1}}{\partial b_1^k} & \cdots & \frac{\partial y_N^{k+1}}{\partial b_N^k} \\ \frac{\partial u_1^{k+1}}{\partial y_1^k} & \cdots & \frac{\partial u_1^{k+1}}{\partial y_N^k} & \frac{\partial u_1^{k+1}}{\partial u_1^k} & \cdots & \frac{\partial u_1^{k+1}}{\partial u_N^k} & \frac{\partial u_1^{k+1}}{\partial c_1^k} & \cdots & \frac{\partial u_1^{k+1}}{\partial c_N^k} & \frac{\partial u_1^{k+1}}{\partial b_1^k} & \cdots & \frac{\partial u_1^{k+1}}{\partial b_N^k} \\ \vdots & \cdots & \vdots & \vdots & \cdots & \vdots & \vdots & \cdots & \vdots & \vdots & \cdots & \vdots \\ \frac{\partial u_N^{k+1}}{\partial y_1^k} & \cdots & \frac{\partial u_N^{k+1}}{\partial y_N^k} & \frac{\partial u_N^{k+1}}{\partial u_1^k} & \cdots & \frac{\partial u_N^{k+1}}{\partial u_N^k} & \frac{\partial u_N^{k+1}}{\partial c_1^k} & \cdots & \frac{\partial u_N^{k+1}}{\partial c_N^k} & \frac{\partial u_N^{k+1}}{\partial b_1^k} & \cdots & \frac{\partial u_N^{k+1}}{\partial b_N^k} \\ \frac{\partial c_1^{k+1}}{\partial y_1^k} & \cdots & \frac{\partial c_1^{k+1}}{\partial y_N^k} & \frac{\partial c_1^{k+1}}{\partial u_1^k} & \cdots & \frac{\partial c_1^{k+1}}{\partial u_N^k} & \frac{\partial c_1^{k+1}}{\partial c_1^k} & \cdots & \frac{\partial c_1^{k+1}}{\partial c_N^k} & \frac{\partial c_1^{k+1}}{\partial b_1^k} & \cdots & \frac{\partial c_1^{k+1}}{\partial b_N^k} \\ \vdots & \cdots & \vdots & \vdots & \cdots & \vdots & \vdots & \cdots & \vdots & \vdots & \cdots & \vdots \\ \frac{\partial c_N^{k+1}}{\partial y_1^k} & \cdots & \frac{\partial c_N^{k+1}}{\partial y_N^k} & \frac{\partial c_N^{k+1}}{\partial u_1^k} & \cdots & \frac{\partial c_N^{k+1}}{\partial u_N^k} & \frac{\partial c_N^{k+1}}{\partial c_1^k} & \cdots & \frac{\partial c_N^{k+1}}{\partial c_N^k} & \frac{\partial c_N^{k+1}}{\partial b_1^k} & \cdots & \frac{\partial c_N^{k+1}}{\partial b_N^k} \\ \frac{\partial b_1^{k+1}}{\partial y_1^k} & \cdots & \frac{\partial b_1^{k+1}}{\partial y_N^k} & \frac{\partial b_1^{k+1}}{\partial u_1^k} & \cdots & \frac{\partial b_1^{k+1}}{\partial u_N^k} & \frac{\partial b_1^{k+1}}{\partial c_1^k} & \cdots & \frac{\partial b_1^{k+1}}{\partial c_N^k} & \frac{\partial b_1^{k+1}}{\partial b_1^k} & \cdots & \frac{\partial b_1^{k+1}}{\partial b_N^k} \\ \vdots & \cdots & \vdots & \vdots & \cdots & \vdots & \vdots & \cdots & \vdots & \vdots & \cdots & \vdots \\ \frac{\partial b_N^{k+1}}{\partial y_1^k} & \cdots & \frac{\partial b_N^{k+1}}{\partial y_N^k} & \frac{\partial b_N^{k+1}}{\partial u_1^k} & \cdots & \frac{\partial b_N^{k+1}}{\partial u_N^k} & \frac{\partial b_N^{k+1}}{\partial c_1^k} & \cdots & \frac{\partial b_N^{k+1}}{\partial c_N^k} & \frac{\partial b_N^{k+1}}{\partial b_1^k} & \cdots & \frac{\partial b_N^{k+1}}{\partial b_N^k} \end{bmatrix} \tag{7}$$

The MLE is defined as

$$\lambda_k = \frac{1}{N} \ln \left| B_{k,N} \right| \tag{8}$$

where $\left| B_{k,N} \right|$ means the determinant of matrix $B_{k,N}$ [13,14]. A positive MLE indicates the instability of the system but its negative amount indicates the stabe system.

On the other hand, the transmission coefficient of the system (T) is given as

$$T = \exp(-2\lambda_k N) \tag{9}$$

where N is the number of base pairs in DNA lattice.

Transmission coefficient is related to the Landauer resistance via

$$\rho = \frac{1-T}{T} \tag{10}$$

in units of the quantum resistance $h/2e^2$ $(\approx 13k\Omega)$ [18].

Results and discussions

By analyzing the *MLE* theory, one could obtain the range of the parameters to have the best ordered field variables[14]. The growth of MLE corresponding to increasing the disorderness of the system then the best range for the parameters of the system is where the *MLE* takes its smaller values, which means that spatial pattern of system is ordered.

Figs. 1(a) and 1(b) show the variation of MLE and Landauer resistance with respect to the temperature in absent the external field, respectively. We have considered the case of homopolymer DNA and a length of N=100 base pairs in our numerical calculations. By considering the figures, we could see the inherently charge transfer in DNA and stability regions of the system even in absent the external current. The minimal value of the MLE and DNA resistance is about where the DNA is denatured $(\approx T = 340 - 350K)$.

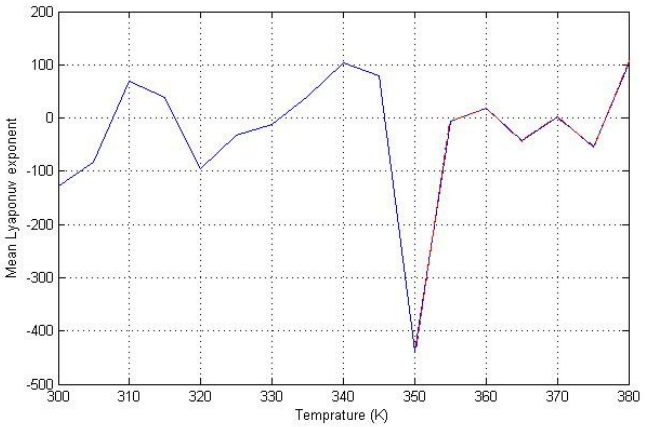

Fig. 1(a). Mean Lyapunov exponent versus the temperature in absent the external field.
$t_0 = 0.4, k = 0.85, \alpha = 0.2, \omega_0 = 0.01, \gamma_0 = 0.01$.

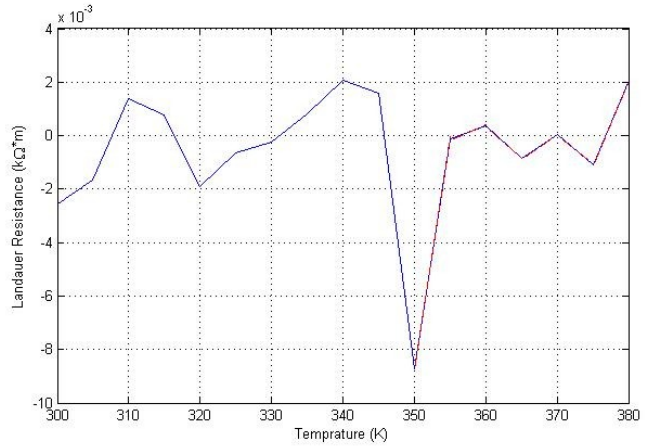

Fig. 1(b). Landauer resistance versus the temperature in absent the external field.
$t_0 = 0.4, k = 0.85, \alpha = 0.2, \omega_0 = 0.01, \gamma_0 = 0.01$.

Following figures appear the effect of external field with different parameters on charge transfer and resistance of DNA. We could see applying the external field decrease the resistance of DNA but the minimal value of resistance is again about where DNA is denatured.

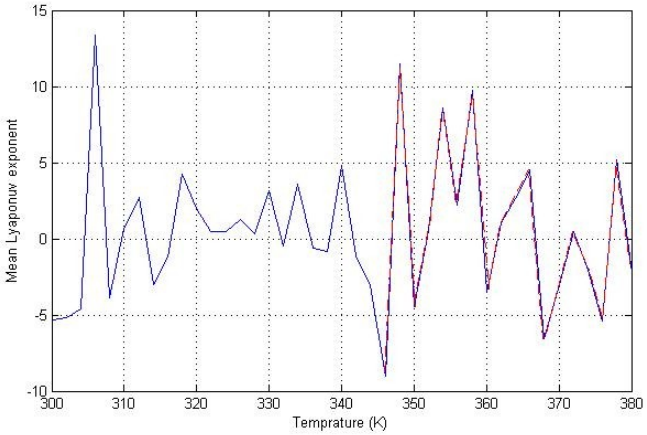

Fig. 2(a). Mean Lyapunov exponent versus the temperature in present the external field. $t_0 = 0.4, k = 0.85, \alpha = 0.2, \omega_0 = 0.01, \gamma_0 = 0.01, E_0 = 10, \omega = 1$.

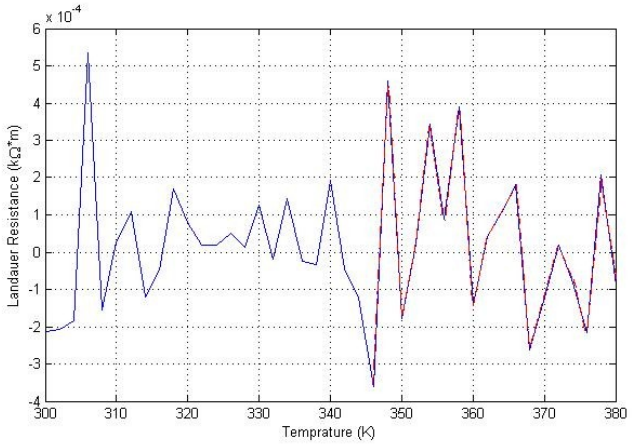

Fig. 2(b). Landauer resistance versus the temperature in absent the external field. $t_0 = 0.4, k = 0.85, \alpha = 0.2, \omega_0 = 0.01, \gamma_0 = 0.01, E_0 = 10, \omega = 1$.

On the other hand, by analyzing the MLE theory the best range for the parameters of the electrical field is selected, as charge current is encountered with minimal resistance.

Figs. 3 and 4 show the variations of MLE and resistance with respect to the field parameters.

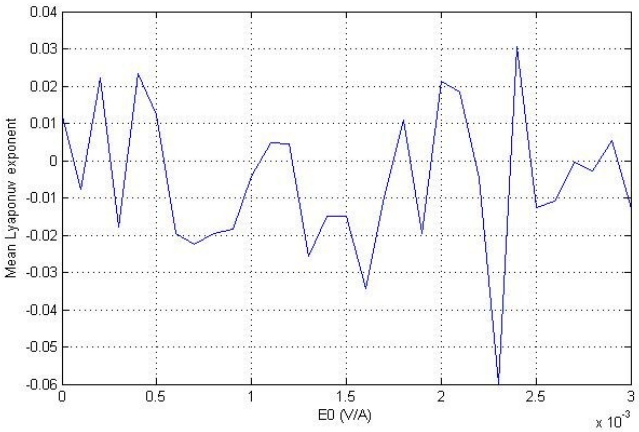

Fig. 3(a). Mean Lyapunov exponent versus the amplitude of the external field.
$t_0 = 0.4, k = 0.85, \alpha = 0.2, \omega_0 = 0.01, \gamma_0 = 0.01, \omega = 1, temperature = 300K$.

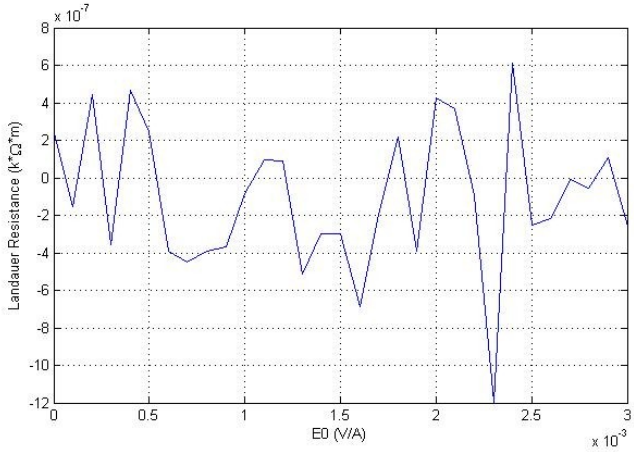

Fig. 3(b). Landauer resistance versus the amplitude of the external field.
$t_0 = 0.4, k = 0.85, \alpha = 0.2, \omega_0 = 0.01, \gamma_0 = 0.01, \omega = 1, temperature = 300K$.

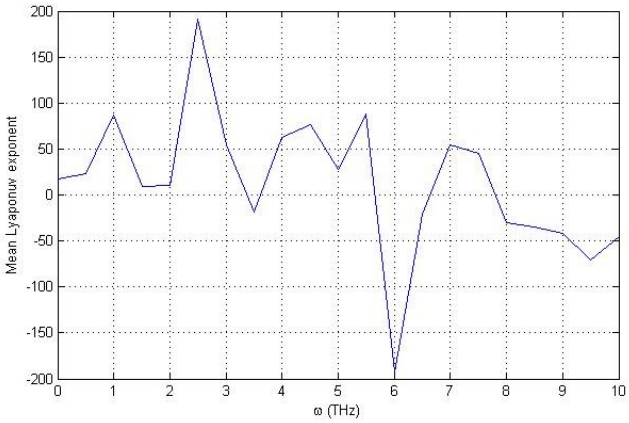

Fig. 4(a). Mean Lyapunov exponent versus the frequency of the external field.
$t_0 = 0.4, k = 0.85, \alpha = 0.2, \omega_0 = 0.01, \gamma_0 = 0.01, E_0 = 2.3\, mV/A, temperature = 300K$.

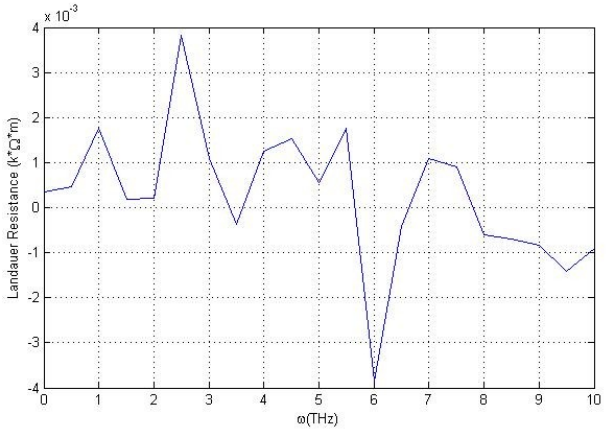

Fig. 4(b). Landauer resistance versus the frequency of the external field.
$t_0 = 0.4, k = 0.85, \alpha = 0.2, \omega_0 = 0.01, \gamma_0 = 0.01, E_0 = 2.3\, mV/A, temperature = 300K$.

3. Conclusions

By considering the MLE, the relation between the system parameters and spatial pattern of the system is evaluated. According to the obtained results, the spatial pattern of the system is varied with respect to the parameters. In the current study, the effect of external field on charge transfer and resistance of DNA is studied. The variation of MLE and thus Landauer resistance with respect to the different parameters such as temperature, amplitude and the frequency of external field are appeared. It becomes apparent that MLE and Landauer

resistance are minimal about where the DNA is denatured. On the other hand, our results show the sensitivity of *MLE* to the field parameters. Then, by considering the MLE, the best range of the system parameters is selected.

References

1. V.A. Malyshev. DNA double helices for single molecule electronics. Physical Review Letters 98: 096801, 2007.
2. S.O. Kelley and J. K. Barton. electron transfer between bases in double helical DNA. Science 283,5400: 375, 1999.
3. T. Cramer and et al. Theory and simulation of DNA charge transfer: From junctions to networks. The Journal of Physical Chemistry B 108: 16586, 2004.
4. B. M. Venkatesan and R. Bashir. Nanopore sensors for nucleic acid analysis. Nature Nanotechnology 6.10: 615, 2011.
5. H.W. Fink and C. Schönenberger. Electrical conduction through DNA molecules. Nature 398.6726: 407, 1999.
6. D. Porath and et al. Direct measurement of electrical transport through DNA molecules. Nature 403.6770: 635, 2000.
7. E. Braun and et al. DNA-templated assembly and electrode attachment of a conducting silver wire. Nature 391.6669: 775, 1998.
8. A. Yu. Kasumov and et al. Proximity-induced superconductivity in DNA. Science 291.5502: 280, 2001.
9. S. Komineas, G. Kalosakas and A. R. Bishop. Effects of intrinsic base-pair fluctuations on charge transport in DNA. Physical Review E 65.6: 061905, 2002.
10. J. Zhu and et al. Local electronic structure in the Peyrard–Bishop–Holstein model. Journal of Physics: Condensed Matter 19.13: 136203, 2007.
11. W. Su, J. R. Schrieffer and A. J. Heeger. Solitons in polyacetylene. Physical Review Letters 42.25: 1698, 1979.
12. W. Su, J. R. Schrieffer and A. J. Heeger. Soliton excitations in polyacetylene. Physical Review B 22.4: 2099, 1980.
13. H. Shibata. Lyapunov exponent of partial differential equation. Physica A: Statistical Mechanics and its Applications 264.1: 226,1999.
14. H. Shibata. Fluctuation of mean Lyapunov exponent for turbulence. Physica A: Statistical Mechanics and its Applications 292.1: 175, 2001.
15. S. Behnia and et al. A novel approach for the potential parameters selection of Peyrard–Bishop model. Physics Letters A 375.7: 1092, 2011.
16. S. Behnia and et al. Mean Lyapunov exponent approach for the helicoidal Peyrard–Bishop model. Physics Letters A 375.41: 3574, 2011.
17. R. Hilborn. Chaos and Nonlinear Dynamics, Oxford University Press, 2000.
18. L.M. Lifshits, S.A. Gredeskul, L.A. Pastur, Introduction to the Theory of Disordered Systems. Wiley, New York, 1988.

Transport properties in the standard map with long time

Lydia Bouchara[1], Ouerdia Ourrad Meziani[2], and Xavier Leoncini[3]

[1] Laboratory of Theoretical Physics, A. MIRA University-Targa Ouzemour 06000, Bejaia, Algeria (E-mail: l.bouchara@yahoo.fr, omeziani@yahoo.fr)
[2] Theoretical Physics Centre, UMR 6207, Aix-Marseille University, Luminy, Case 907 F-13288 Marseille cedex 9, France (E-mail: xavier.leoncini@univ-amu.fr)

Abstract. Anomalous diffusion was distinguished by the behavior of the maximum of distributions of v_n that can be described by a new exponent α. The existence of a characteristic exponent $\alpha \neq 1/2$ imply the anomalous transport, moreover if $\alpha > 1/2$ we expect a sub-diffusive transport and if $\alpha < 1/2$ we expect a superdiffusive transport.

Keywords: Dynamical system, Hamiltonian chaos, Anomalous transport.

1 Introduction

Anomalous transport refers to non equilibrium processes that can not be described by using standard methods of statistical physics Zaslavsky [1], Leoncini & Zaslavsky [2]. The theoretical description of such different phenomena leads, in turn, to the prediction of novel physical and mathematical properties such as sub and super diffusion that can be described by an exponent α Leoncini & al.[3]. In Bouchara & al.[4] we have shown that transport in the standard map can be multifractal. In this work we show you the nature of transport for the long time in the case of the standard map for two parameter of control $k=10$ and $k=1.5$. Recall that, The transport in Hamiltonian systems has been already studied by

7th CHAOS Conference Proceedings, 7-10 June 2014, Lisbon Portugal
C. H. Skiadas (Ed)

Chirikov [5], Venegeroles [6], Mackay & al [7], Karney [8] Lichtenberg & Lieberman [9] (and many others). We often seek to achieve a very long time to have a general idea about the nature and behavior of the transport.

2 Standard map

The standard map arises naturally as a Poincaré mapping of the kiked rotor model. Whose Hamiltonian write

$$H = \frac{p^2}{2} - w_0 \cos q \sum_{n=-\infty}^{+\infty} \delta(t - n\tau) \quad (1)$$

Where w_0 is somme frequency, τ somme characteristic period and δ is the Dirac function. We will consider the motion on the torus. The equations of the standard map are writes:

$$p_{n+1} = p_n + k\sin q_n \left[2\pi\right] \quad (2)$$

$$q_{n+1} = q_n + p_{n+1} \left[2\pi\right] \quad (3),$$

where k is parameter that characterizes the force amplitude [5], [6]. The chaos takes over as k grows.

2 Results

We consider two cases when $k = 10$ and $k = 1.5$ and can through consider an analog of the norm of the phase space speed

$$v = \left(k^2 \sin^2 q + p^2\right)^{1/2} \quad (4)$$

we shall now consider the average of v along a typical trajectory. The probability density of the distribution of the average of v represented respectively for $k = 10$ and $k = 1.5$ in the figure 1.

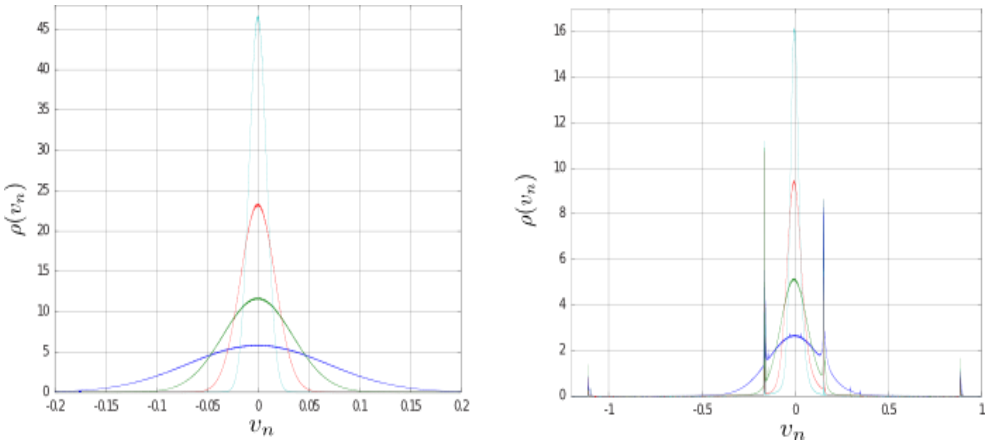

Figure 1. Distributions of v_n for flatest to thinest $n = 10^3, 8\times10^3$, $3.2\times10^4, 1.28\times10^5$ .Left : $k = 10$ Right : $k = 1.5$.

We consider the distribution of finit time averages. This means that we shall compute averaves of v over finite times. Leoncini & al [3] directly have relation between the second moment μ and the new parameter α which write

$$\alpha = 1 - \mu/2 \tag{5}$$

If $\alpha \neq 1/2$ the transport is anomal, moreover

- if $\alpha > \frac{1}{2}$ the transport is subdiffusive
- if $\alpha < \frac{1}{2}$ the transport is superdiffusive

else if $\alpha = 1/2$ the transport is diffusive.

In our cases the transport is found to be regular and diffusive in the case $k = 10$ with α =1/2 with long times. In the case $k = 1.5$ the transport is found to be superdiffusive with a characteristic exponent α =0.38 (Figure 2).

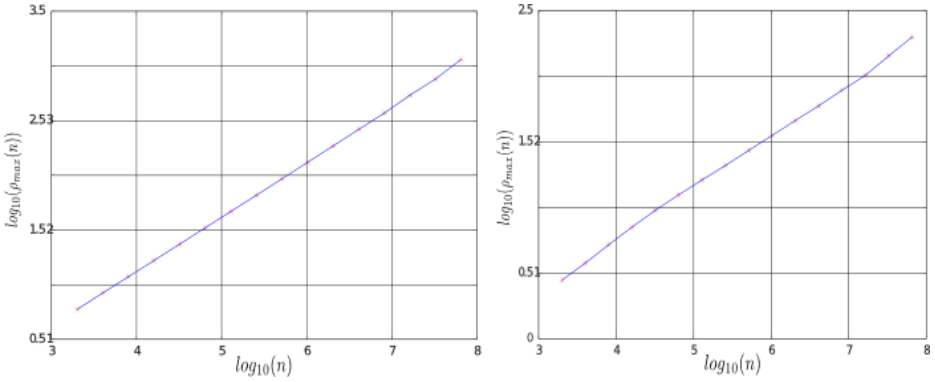

Figure 2. Evolution of $\rho_{max}(n)$ versus n in logarithmic scale. Left : $k = 10$ Right : $k = 1.5$.

3 Conclusion

The transport is found superdiffusive with $\alpha < 1/2$ for the case $k=1.5$, wich correspond to situation of mixed phase. The Gaussian transport for the fully chaotic regime is giving with $\alpha = 1/2$. Using the most known parameter α conveys good information relative to the nature of the transport. We find that the nature of the transport, in considered cases, is similar in Bouchara & al [4] by using parameter μ.

References

1. G.M. Zaslavsky, Hamiltonian chaos and fractional dynamics, Oxford University Press 2005,
2. X. Leoncini, G.M. Zaslavsky, Jets, stickness, and anomalous transport, Phys. Rev E, volume 65, 046216 (2002)
3. X. Leoncini, C. Chandre et O. Ourrad, Ergodicite, collage et transport anomal, Elsevier science, 530-535. In *Comptes Rendus Mécanique* 336 (6).2008,
4. L.Bouchara, O. Meziani, X. Leoncini, Multifractal transport in the standard map, AIPConf.Proc1444, 476 ; doi : 10.1063/1.4715481, 2012

5. B. Chirikov, Phys. Rep 52, 263-379 , 1979.
6. Roberto Venegeroles, Universality of Algebraic Laws in Hamiltonian Systems, PRL 102, 064101 (2009) PHYSICAL REVIEW LETTERS 13 FEBRUARY 2009
7. R. S. Mackay, J. D. Meiss and I. C. Percival, Transport in hamiltonian systems, Physica 13D, 55-81 North-Holland, 1984
8. Charles F.F. Karney, Long-time correlations in the stochastic regime, Physica 8D (1983) 360-380 North-Holland Publishing Company
9. A. Lichtenberg and M. Lieberman, Regular and Chaotic Dynamics, Springer, N.Y. 1992,

Microscopic reaction diffusion patterns generated in nanometer size confinements

Jorge Carballido-Landeira* and Alberto P. Muñuzuri

Universidad de Santiago de Compostela, Santiago de Compostela, Spain
*E-mail: jorge.carballido@gmail.com

Abstract: The Belousov-Zhabotinsky (BZ) reaction is one of the most studied reaction-diffusion systems able to display periodic oscillations when continued stirred and target patterns and/or spirals in spatially extended systems. Once the BZ reaction is placed inside nanometric micelles surrounded by an anionic surfactant and dispersed in an oleic system, the variety of spatial patterns increase considerably. The diversity on pattern formation is originated by the two different diffusion mechanisms available depending on the reagents charge nature. Non-polar chemicals may diffuse through the membrane and into the octane while polar chemicals diffuse within the entire nanodroplet, almost two orders of magnitude slower. On changing the confinement conditions where the BZ reaction takes place, the BZ-AOT system is able to present different dynamics, ranging from Turing structures (such as spots, stripes or labyrinthine) to standing waves, antispirals and packet waves.

Keywords: Reaction Diffusion systems. Belousov-Zhabotinsky reaction. Active microemulsion.

1. Introduction

The Belousov-Zhabotinsky (BZ) reaction is considered a prototype system for studies of reaction–diffusion phenomenon. This oscillatory chemical reaction involves the bromination and consequently oxidation of an organic substrate (originally citric acid) by bromate ions immersed into a strongly acidic solution [1]. Typically the catalysts used in the BZ reaction are cerium or ferroin, but the presence of ruthenium bipyridyl [$Ru(bpy)3^{+2}$] complex has demonstrated photosensitive features in the BZ reaction. The presence of a redox indicator exhibiting different colors in the reduced and oxidized state of catalyst helps to visualize periodical temporal oscillations while the reaction is continuously stirred or spatiotemporal patterns when the reaction is kept unstirred [2].

7th CHAOS Conference Proceedings, 7-10 June 2014, Lisbon Portugal
C. H. Skiadas (Ed)

The possibility to encapsulate the BZ reaction into nanodroplets of nanometric micelles bridges the gap between reaction diffusion systems and the effects of confinements. Thus, the BZ reagents are confined into nanometer-sized aqueous droplets surrounded by a surfactant monolayer and soaked in a continuous hydrophobic phase (octane). Here, the polar surfactant heads are orientated inwards (towards the droplet core), while the hydrophobic tails face the oil continuous phase [3].

There are two important parameters that define the reverse microemulsions. One of them is the hydrodynamic radius of the nanodroplets (R_d), which is defined as the addition of the size of the surfactant monolayer and the water nanodroplet core (Rw) [4]. The former is determined by the surfactant size (typically the anionic sodium bis(2-ethylhexyl) sulfosuccinate also known as AOT) and the latter is proportional to the molecular ratio between the aqueous and oil phase (ω_0):

$$R_w = 1.7\omega_0$$

The other main characteristic is the volume fraction of the water phase, defined as

$$\phi_w = V_W \Big/ (V_W + V_O)$$

where Vw and Vo are the volume of the aqueous and oil phases of the system. of the micro-emulsion system. These properties of the micro-emulsion have a direct influence in the measurable features of the BZ reaction [5-7]

The so-called BZ-AOT system presents two different diffusive mechanisms of the chemical components. Polar BZ reagents are confined into the aqueous phase of the reverse microemulsion and diffuse with the water nanodroplets. The diffusion coefficient is then determined by the Stokes-Einstein equation:

$$D_d = K_B T \Big/ 6\pi\eta R_d$$

where K_B, T, η are Boltzmann constant, the absolute temperature and the viscosity of the solvent, respectively.

In the course of the reaction several nonpolar intermediates are generated These non-polar chemicals are able to diffuse through the membrane and into the oleic phase as single molecules with exhibiting diffusion coefficients almost two orders of magnitude faster than usual nanodroplets. Among the intermediates are the Br_2 and BrO2, which are known as fast-diffusing inhibitor and fast-diffusing activator, respectively [3].

2. The Model and Simulations

In order to model the main characteristics of the BZ-AOT system, Vanag and Epstein have proposed a variation of the well-known Oregonator model [8]. Thus, their model accounts those species able to migrate into the oleic phase in addition to the "ordinary" chemical reactions occurring in the aqueous compartments. The dynamics achieved in the BZ-AOT system can be expressed by the following set of differential equations [3]:

$$\frac{\partial x}{\partial \tau} = F(x,z,s,u) + D_x \Delta x \tag{1}$$

$$\frac{\partial z}{\partial \tau} = G(x,z,s,u) + D_z \Delta z \tag{2}$$

$$\frac{\partial s}{\partial \tau} = H(x,z,s,u) + D_s \Delta s \tag{3}$$

$$\frac{\partial u}{\partial \tau} = K(x,z,s,u) + D_u \Delta u \tag{4}$$

with

$$F(x,z,s,u) = -fz\frac{(x-q)}{(x+q)} + x(1-\beta) - x^2 + s$$

$$G(x,z,s,u) = x - z(1+\alpha) + \gamma u + D_z \Delta z$$

$$H(x,z,s,u) = \frac{1}{\varepsilon_1}(\beta x - s + \chi u) + D_s \Delta s$$

$$K(x,z,s,u) = \frac{1}{\varepsilon_2}(\alpha z - \gamma u) + D_u \Delta u$$

where x,z are the dimensionless concentrations of $HBrO_2$ and the catalyst of the reaction (i.e. ferroin, Ru(bpy), cerium), while s and u are the species soluble into the oleic phase: the inactive form of activator (BrO2) and the inhibitor (Br_2), respectively. To account the differences in the diffusion rates we used $D_s=D_u >> D_x=D_z$

The homogeneous steady state concentrations can be achieved by finding the solutions of the equations (1)-(4) once the temporal and spatial derivatives are setted to zero, *i.e.*, by solving F(x,z,s,u)=0, G(x,z,s,u)=0, H(x,z,s,u)=0 and K(x,z,s,u)=0. The stability of each one of the possible steady states will be determined by the eigenvalues obtained through the characteristic equation [9]:

$$\det(\mathbf{A} - \lambda\mathbf{I} - k^2\mathbf{D}) = 0$$

where **I** is the identity matrix, **D** is the matrix of the diffusion coefficients here consider diagonal (neglecting cross-diffusion effects (even though they have been experimentally observed in the BZ-AOT systems) and **A** is the Jacobian matrix of equations (5)-(6):

$$A(x,z,s,u) == \begin{vmatrix} \left(1-\beta-2x-\frac{f(q-x)z}{(q+x)^2}-\frac{fz}{(q+x)}\right)/\varepsilon & f(q-x)/(\varepsilon(q+x)) & 1/\varepsilon & 0 \\ 1 & -1-\alpha & 0 & \gamma \\ (\beta/\varepsilon_2) & 0 & -(1/\varepsilon_2) & \chi/\varepsilon_2 \\ 0 & \alpha/\varepsilon_3 & 0 & -\gamma/\varepsilon_3 \end{vmatrix}$$

We observed that although Turing and Hopf instabilities may coexist in our range of parameters, the predominant mode differs according to the diffusion coefficient ratio (Figure 1). Thus, when the diffusion coefficient of the non-polar species is almost two-fold larger than the diffusion of the entire nanodroplet the dispersion relationship exhibits a predominant Turing mode slightly predisposed by Hopf domain (purple curve in Figure 1). However, decreasing the ratio of diffusion coefficients the Hopf mode prevails (red curve) until the Turing mode vanishes (black curve).

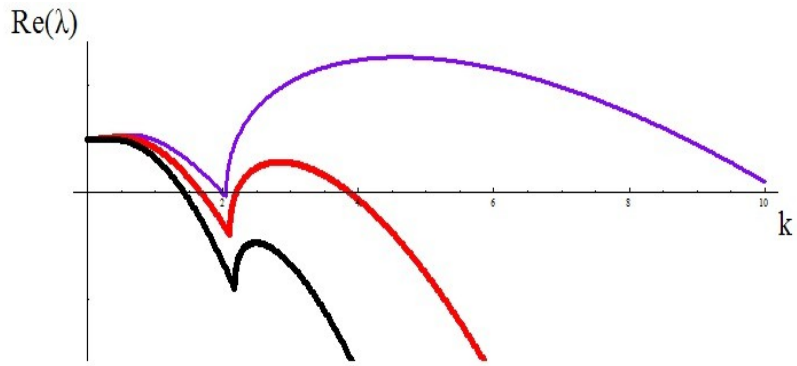

Figure 1. Dispersion relations exhibiting the interaction between the Turing and Hopf instabilities for different ratios between nonpolar intermediates and polar species confined in the microemulsion (Ds/Dx):80 (violet curve), 40 (red), 8 (black) . The model parameters to obtain this dispersion relations are α=8;

β=0.34; γ=0.2; χ=0.;□1.1;□0.001; ε=0.37; εs2=1.5; ε3=0.006;

Initially, we will consider the set of equations (1)-(4) in the absent of diffusion, *i.e.* without special considerations. This case resembles those reactions carried out under continuously stirring conditions in beakers. To do that, we use an Euler method with a time step of 0.01 time units (t.u.). Under these conditions, the BZ-AOT model exhibits an oscillatory solution with a characteristic period. Figure 2 (top) demonstrates this periodically behavior of the species concentration oscillating between a maximum and a minimum values.

Once diffusion was considered, simulations of equations (1)-(4) were performed by a Dufort-Frankel method in addition to Dirichlet and Newman conditions:

$$x(\bar{r},t)\big|_{t=t_0} = x_{ini} \quad ; \quad \hat{n}\nabla x\big|_{\partial\Omega} = 0$$
$$z(\bar{r},t)\big|_{t=t_0} = x_{ini} \quad ; \quad \hat{n}\nabla z\big|_{\partial\Omega} = 0$$
$$s(\bar{r},t)\big|_{t=t_0} = s_{ini} \quad ; \quad \hat{n}\nabla s\big|_{\partial\Omega} = 0$$
$$u(\bar{r},t)\big|_{t=t_0} = u_{ini} \quad ; \hat{n}\nabla u\big|_{\partial\Omega} = 0$$

Under Turing conditions (violet curve in Figure 1) we observed stationary patterns separated an equidistant wavelength. In Figure 2 (left panel) we show two characteristic Turing structures obtained by tunning the model parameters. The white (black) color in these figures stands for a high (low) concentration of the oxidized catalyst. Both kind of Turing patterns, spots and stripes, are experimentally achieved in the BZ-AOT system once the active micro-emulsion is sandwiched between two optical windows (Figure 2 right panel). The similitude between numerical and experimental patterns suggests that model (1)-(4) is a good candidate to display those structures obtained in the BZ-AOT system.

In addition to stationary Turing structures, the BZ-AOT system exhibits a rich variety of dynamics not possible without the confinement into nanodroplets, such as dashed waves, standing and packet waves, oscillons, segmented waves, etc [10-13]

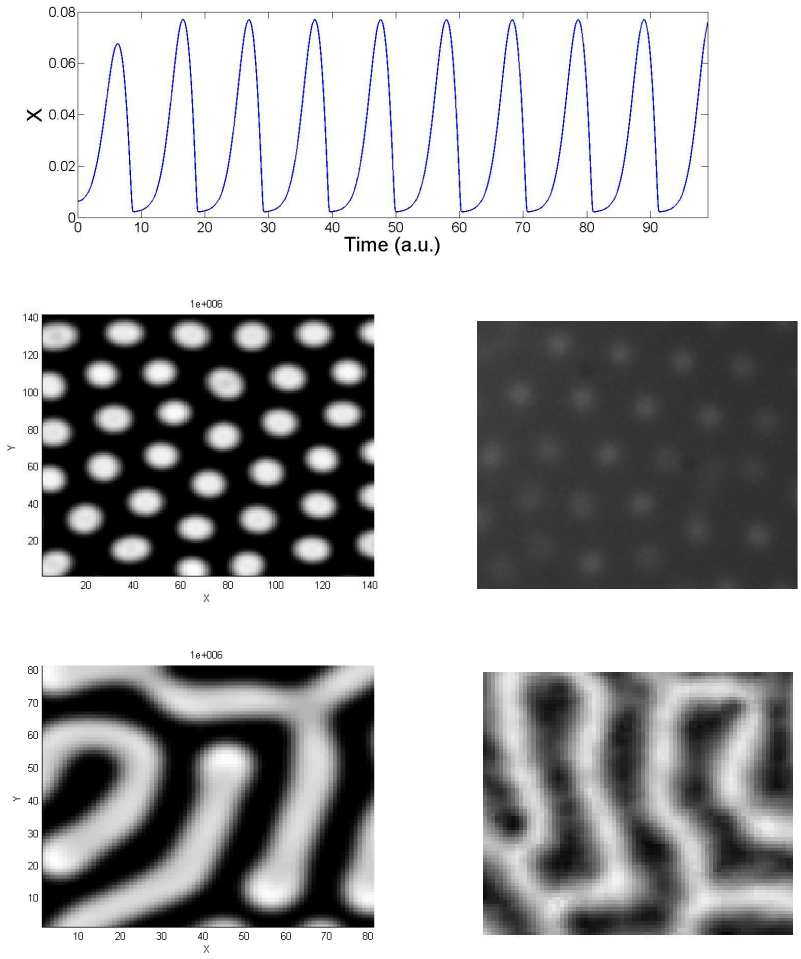

Figure 2. Model simulations of equations (1)-(4). Top: periodically temporal oscillations obtained in absence of diffusion. Middle and bottom: Two dimensional structures achieved numerically (left panel) and the comparative with experimental results (right panel) .

3. Conclusions

.The confinement of a chemical oscillator into a micro-emulsion system generates a variety of spatial patterns not accessible without the compartmentalization. The diversity on pattern formation is understood by the presence of two different diffusion mechanisms. While Non-polar species may diffuse into the oleic phase, polar reagents are restricted to diffuse inside the nano-droplet system, being their diffusion coefficient considerably slower. The differences in the diffusion coefficients have been accounted by a four variable model, composed by two fast-diffusing species and two slow ones. We demonstrate the presence of Turing structures, which are patterns stationary in time with a characteristic spatial wavelength. Furthermore, we also present experimental results that qualitatively agree with our numerical simulations, validating our four variable model. It is remarkable to mention that there are several models to represent compartment active systems. They are have been indiscriminately used to characterize the arising of new dynamics as well as the influence of external forcing into the well-known patterns [14-18]. Recently, cross-diffusion of the chemical reactants was considered one of the probable mechanisms to achieve such diversity of pattern formation and has been added to the model scheme [19**].**

References

1. B. P. Belousov, *Collected Abtracts on Radiation Medicine*.Moscow:Medgiz: A. V. Lebedinskii. Page 145 (1959.)
2. A.N. Zaikin, and A. M. Zhabotinsky,. *Nature (London)*, 225, 535. (1970)
3. V. K. Vanag, Phys.-Usp., 2004, 47, 923–941.
4. A.M. Cazabat, D. Langevin, D. and D.Pouchelon, . *J. Colloid Interface Sci.*,73, 1. (1980)
5. V.K. Vanag, and D.V. Boulanov, . *JPhys. Chem.*,1998, 1449 (1994)
6. E. Villar-Alvarez, *et al.* The Journal of Chemical Physics,134 094512 (2011)
7. J. Carballido-Landeira, P. Taboada and A. P. Muñuzuri, , Phys. Chem. Chem. Phys., 13,4596, (2011)
8. R.J. Field, and R.M. Noyes, *J. Chem. Phys.*,60,1877 (1974)
9. Strogatz, S. 1994. *Nonlinear Dynamics and Chaos*. Massachusetts: Perseus Books.
10. V. K. Vanag and I. R. Epstein, Phys. Rev. Lett. **87**, 228301 (2001).
11. *J. Carballido-Landeira et al.* , Phys. Chem. Chem. Phys., 10,1094-1096, (2008)
12. V. K. Vanag and I. R. Epstein, Phys. Rev. Lett. **88**, 088303 (2002).
13. V. K. Vanag and I. R. Epstein Phys. Rev. Lett 92, 128301 (2004)
14. J. Guiu-Souto *et al*. , Phys. Rev. E,82, 066209, (2010)
15. J. Carballido-Landeira, V. K. Vanag and I. R. Epstein, Phys. Chem.Chem. Phys,12, 3656-3665, (2010)

16. A. Kaminaga, V.K. Vanag, and I.R. Epstein. *Angew. Chem. Int. Ed.*,118, 3159–3161.(2006)
17. J. Guiu-Souto *et al., Soft Matter,DOI: 10.1039/c3sm27624d (2013)*
18. J. Carballido-Landeira, P. Taboada and A. P. Munuzuri, Soft Matter, 8, 2945 (2012)
19. V. K. Vanag, F. Rossi, A. Cherkashin, and I. R. Epstein, J. Phys. Chem. B **112**(30), 9058 (2008).

Bottom Particles Segregation: Experiments and Numerical Simulations Using Non-linear Diffusion Equation.

Tien Dat Chu, François Marin, Armelle Jarno-Druaux

UMR CNRS 6294, University of Le Havre, Le Havre, France

Djillali Tiguercha, Anne-Claire Bennis, Alexander B. Ezersky

UMR CNRS 6143, University of Caen and Basse Normandie, Caen, France
E-mail: Alexandr.Ezersky@unicaen.fr

Abstract: We report experimental and theoretical results on segregation of particles in sandy bottom under the action of oscillating velocity field due to surface waves. Experiments were performed in-situ and in wave flume. Segregation in the mixtures of light and heavy particles of the same diameter and small and large particles of the same density was observed. It was found that segregation appears on the background of sand ripples generation in the upper «active» zone of the bottom. The thickness of this zone is proportional to the amplitude of velocity oscillation. The topology of segregation patterns depends on particle size differences, on particle density differences as well as on particle percentage composition in the mixture. It was revealed that small particles with small percentage are concentrated below sandy ripples crest. If percentage composition of small and large particles are approximately equal, the large particles are concentrated below the ripples crests. Light particles quite the «active» zone where concentration of heavy particles increases. To investigate the segregation of particles we use non-linear diffusion equations in the presence of gravity field like it was done recently in paper of Fernandez *et al* (Physica A, 2003, 327, 94–98). The main idea of this model is to take into account the different sizes and densities of particles using mobility coefficients in diffusion equations for concentration of particles. We extended one dimensional model of Fernandez *et al* for two dimensional case. Numerical simulations demonstrate good qualitative coincidence with experimental data. In particular, zones with high concentration of small and large particles below ripples crest were obtained in numerical simulations depending on percentage composition of particles. Formation of the layer where the concentration of light particles sufficiently decreases was also found in numerical simulations. Importance of segregation processes for biological and environmental problems is discussed.

Keywords: Segregation, sand ripples, surface wave, sea bottom, non-linear diffusion equation.

1. Introduction

Interest in segregation of particles is associated with a large number of different practical applications. For example segregation is widely used to sort materials

7th CHAOS Conference Proceedings, 7-10 June 2014, Lisbon Portugal
C. H. Skiadas (Ed)

in the mineral processing and building industries. To date, the most thoroughly studied patterns are the ones that result from the segregation in a dry mixture of solid particles with different properties: size, density, and shape. The process of segregation occurs in the mixture of particles subjected by an external field. It can be vibration, gravity forces, rotation, or another external influence. It should be noted that under the influence of external fields, one could observe the appearance of segregation more often than mixing. Mixture of particles in external field can be considered as a non-equilibrium dissipative media that is far from equilibrium. Spatially homogeneous state in this media may be unstable. As a result of this instability of mixture of particles spatial patterns appear. The dynamics of these patterns has been investigated for granular materials when interaction of particles includes a dry friction. This paper is devoted to pattern formation in a mixture of solid particles immersed in a viscous fluid. It should be noted that the number of studies on segregation pattern formation in such systems is sufficiently small. However, these problems appear very important for different processes that take place on the ocean bottom. It is obvious that such segregation is significant for understanding the problems of sediment transport and erosion of the seabed. The segregation may also lead to the redistribution of micro-and meso benthos on the seabed. Segregation of particles is important for environmental issues, because concentration pattern formation can lead to an abnormally high localization of a particular type of particles in limited areas where conditions can change significantly for the flora and fauna on the seabed. This paper aims to examine the conditions under which it is possible to observe the segregation of particles on the seabed and to investigate the characteristics of emerging patterns on the bottom. The paper is organized as follows. At the beginning some experimental results on particle-size and particle-density segregation are presented. Then we discuss a theoretical model describing segregation and present some results of numerical simulations. Numerically obtained results are compared with experimentally observed patterns.

2. Experimental results

Experiments were conducted in a 10.7-m-long, 0.5-m-wide wave flume [1]. Surface waves are generated by an oscillating paddle at one end of the flume; an absorbing beach is located at the other end (Fig.1). The water depth at rest h is 0.24 m. The height and the period of the wave are measured with two resistive probes. Ripples were generated on the bottom from an initially flat bed, which consisted in a 4-cm layer of mixtures. Two kinds of mixtures were used: for the first mixture (mixture 1): sand of density $\boldsymbol{\rho_1 = 2.65\ 10^3\ Kg/m^3}$, diameter $\boldsymbol{d1=0.17mm}$ and polyvinyl chloride (PVC) grains of density $\rho_{2_2} = 1.35\ \boldsymbol{10^3}$ kg.m^{-3}, median diameter $\boldsymbol{d_1=0.17mm}$. The volume concentration for this mixture are $\boldsymbol{C_1=96\%,\ C_2=4\%.}$ For the second mixture (mixture 2), we used yellow sand with the following properties: $\boldsymbol{d_1= 0.34\ mm,\ \rho_1 = 2.65\ 10^3\ Kg/m^3}$, and red sand: $\boldsymbol{d2=0.15mm,\ \rho_2 = 2.5\ 10^3\ Kg/m^3}$; the volume concentrations were $\boldsymbol{C_1=90\%, C_2=10\%}$ in this case.

Patterns appearing on the bottom are shown in Fig.2. Observations of segregation patterns were possible since the side walls were made of glass and the particles with different properties had different colors. Fig. 2 shows the patterns arising from homogeneous mixtures (Fig. 2ac) of particles under the influence of surface waves. In both mixtures , ripples with spatial period of 10 cm and height 2 cm formed rapidly along the flume once the wave maker was

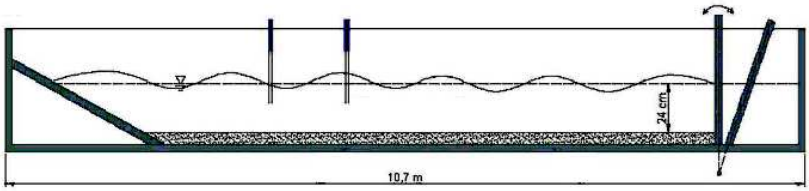

Fig.1 Experimental set-up

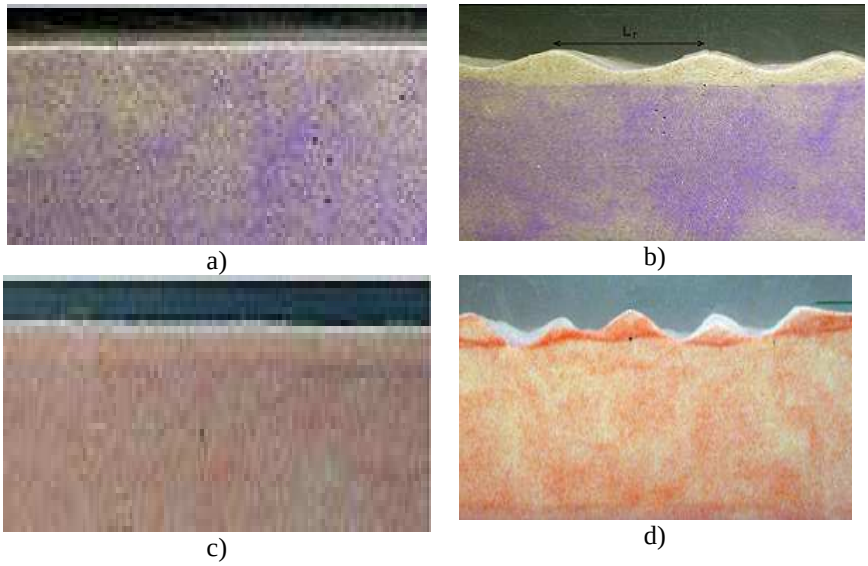

Fig. 2 Segregation patterns appearing from homogeneous mixtures: a) mixture of sand and PVC, b) pattern in mixture (a) appearing after sand ripples generation, c) mixture of yellow sand and red sand, d) pattern in mixture (c) appearing after sand ripples generation.

switched on. The size and shape of ripples were approximatly the same along the flume. For the first type of mixture, a layer where concentration of PVC is very low appeared near the boundary between sand and water (Fig. 2ab). For the

second type of mixture, the segregation resulted in an increase of concentration of red sand (the finest sand in mixture 2) under the ripples crest (Fig.2cd). It should be emphasized that the generation of sand ripples at the bottom is a quite fast process (characteristic time: tens of minutes), whereas the segregation patterns are forming during several hours.

3. Theoretical model.

To describe the particle segregation by currents induced by surface waves, we use the approach developed in [2,3]. A mixture of particles is considered as a gas with a temperature T that is in the field of potential forces. To a mixture of particles can be calculated the entropy S and free energy F: $F=U-TS$, where U is potential energy. The volume concentrations $C_{1,2}$ of particles may be found using variation derivatives of functional $\Im$ [2,3]:

$$\Im=\int F dQ$$

$$\frac{\partial C_{1,2}}{\partial t} + \nabla\cdot\vec{J}_{1,2}=0\,,\ \vec{J}_{1,2}= -\Gamma_{1,2}\nabla\mu_{1,2}\,,\ \mu_{1,2} = \frac{\delta\Im}{\partial C_{1,2}}$$

where $\mu_{1,2}$ are chemical potentials and $\Gamma_{1,2}$ are mobilities of particles.

In these equations particle mobilities $\Gamma_{1,2}$ are not defined. In [2,3] a phenomenological mobility depending on the concentration is used to calculate the concentration of particles. The basic assumption is that there is some limit particle concentration above which the mobility of the particles is zero. Physically, this means that there is a dense packing of particles which totally eliminates their movement. The mobility may be presented as:

$$\Gamma_{1,2}=\Gamma_0 C_{1,2}\Theta(C_c^{1,2}-(C_1+C_2))\cdot\left(1-(C_1+C_2)/C_c^{1,2}\right)^{\Phi_{1,2}}$$

where $\Phi_{1,2}$ are constants discussed in [2,3].

After these assumptions, the non-linear diffusion equation (NLDE) was found for particle concentrations. In [2] segregation of particles was investigated in a one-dimensional case, when the concentrations depend on vertical coordinate z and on time t: $C_{1,2}=C_{1,2}(z,t)$. It was found that NLDE could describe the effect of Brazil nuts: vibrations of particle mixture leads to the fact that larger particles tend to settle over small ones. A qualitative explanation of this effect is quite simple: the small particles fall between large particles.

In the case of sand ripples the problem is much more complicated, because the system is fundamentally two-dimensional. Experiments have shown that the appearance of sand ripples develops much faster than the process of particle segregation. Therefore, for the correct application of the NLDE it is necessary to take into account the sand ripples. How to take into account the

existence of sand ripples in NLDE? Imagine that there is a border between oscillating water and sand ripples. The sandy bottom is a porous medium, where the correlation between the velocity field $\vec{V}$ and pressure field p is determined by Darcy law [4]: $\vec{V} = -\frac{K}{\rho\nu}\nabla p$, where K is the permeability of the porous medium, ρ the water density and ν the kinematics viscosity.

In the sand layer, under the action of oscillating velocity a mean pressure field P is generated. For small amplitude a of sand ripples this mean pressure field may be calculated as:

$$P = \frac{1}{2}\rho U_a^2 ak\cos(kx)\cdot\exp(k(z-h))$$

where a is for amplitude of sand ripples, U_a is the amplitude of oscillating velocity field near the bottom, h the average sand height (see Fig.3), and k the wave number of sand ripples.

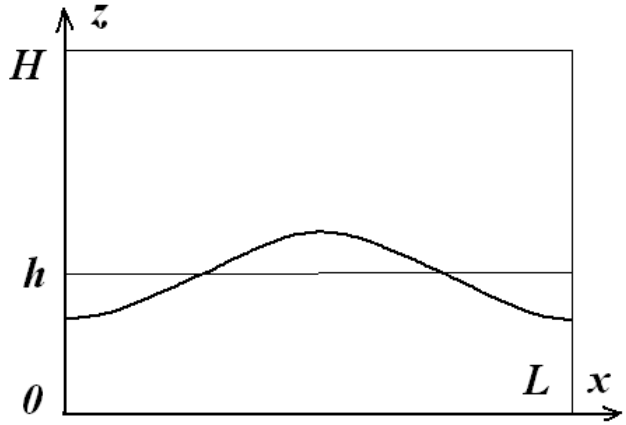

Fig.3 Schematic represatation of integration domaine ($0<x<L$, $0<z<H$) and the boundary between water and sand, $z=h$ corrsponds to the averaged level of the bottom.

The mean force caused by the pressure field acting on a particle with diameter d is expressed as $\vec{F} = -\frac{1}{6}\pi d^3\nabla P$, whereas the component of the force due to the velocity field is zero. The mean pressure may be considered as potential depending on horizontal and vertical coordinates. For our two dimensional case, NLDE concentrations of particles can be described by the following equation:

$$\frac{\partial C_i}{\partial t} = \frac{\partial}{\partial z}\left[\Gamma_i\left(\frac{1}{C_i}\frac{\partial C_i}{\partial z} + \frac{1}{1-C_1-C_2}\left(\frac{\partial (C_1+C_2)}{\partial z}\right)+\gamma_{i,z}\right)\right] +$$

$$\frac{\partial}{\partial x}\left[\Gamma_i\left(\frac{1}{C_i}\frac{\partial C_i}{\partial x} + \frac{1}{1-C_1-C_2}\left(\frac{\partial (C_1+C_2)}{\partial x}\right)+\gamma_{i,x}\right)\right], \; i=1,2$$

$$\gamma_{i,z}=-\frac{4\pi d_i^3}{3k_BT}\left(\frac{\partial P}{\partial x}\right), \quad \gamma_{i,z}=-\frac{4\pi d_i^3}{3k_BT}\left(g(\rho_i-\rho_w)+\frac{\partial P}{\partial z}\right),$$ where ρ_w is for water density, k_B is Boltzmann constant, T is effective temperature of particle mixture

Using this system of equations with boundary conditions at $x=0,L$ and $z=H$, different regimes of particle segregation have been found.

4. Numerical results.

Since the onset of sand ripples in the experiments occurs much faster than the segregation of particles, the initial conditions for the numerical simulations correspond to periodic sand ripples of final amplitude in homogeneous mixture (Fig. 5). We suppose that structure is periodic along x coordinate and $\frac{\partial C_{1,2}(x=0,1)}{\partial x}=0$. For vertical coordinate z conditions of zero particle flux $\frac{\partial C_{1,2}(z=0,1)}{\partial z}=0$, or constant concentration $C_{1,2}(z=0,1)=0$ are used. . The evolution equations for the volume concentrations are discretized with the finite difference method and an explicit time scheme is used.

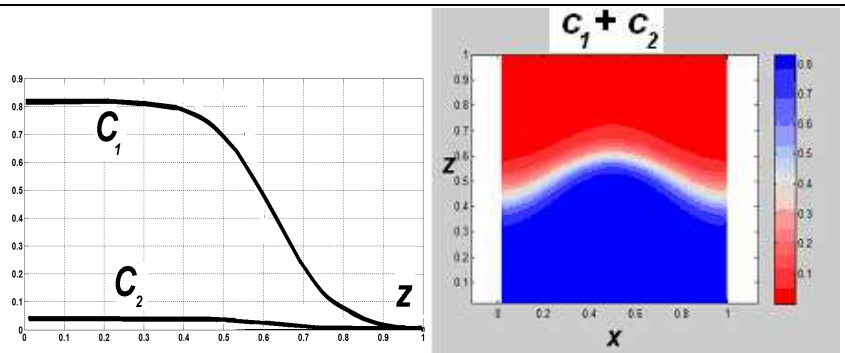

a) Initial conditions of particle concentrations under the crest of ripples

b)Total concentration of particles

Fig. 5

The first series of experiments was performed to model the segregation in the mixture of sand PVC particles. In these experiments parameters $\Phi_{1,2}$ determined by dimensions of particle are equal $\Phi_{1,2}=3.1$, as it was done in [2,3]. Critical concentration of particles above which mobility is zero was $C_{cr}=0.84$. Results are presented in Fig. 6. The main feature of final steady concentration is the following. In the upper part of sand layer *x>0.52* (this point is indicated by an arrow in Fig.6c) the concentration of light (PVC) particles decreases sufficiently in comparison with initial concentration Fig.6c. This pattern may be compared with pattern presented in Fig. 2ab. The concentration of PVC in the layer corresponding non-zero mobility deceases with time.

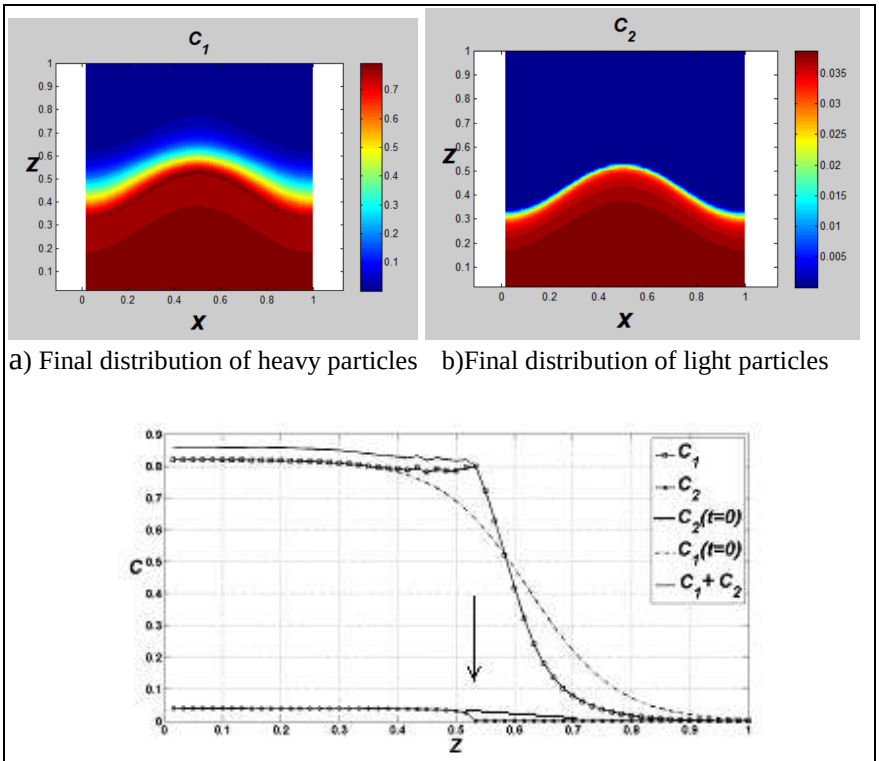

a) Final distribution of heavy particles b)Final distribution of light particles

c) Dependence of particle concentrations on vertical coordinate z under the crest of sand ripples x=0.5

Fig. 6

The second series of experiments was performed to model segregation in the mixture of sand particles with different diameters. In this case, we have

the following values of the parameters $\Phi_1=4$, $\Phi_2=2$, $d_1=1{,}33d_2$. Results are shown in Fig.7. Segregation leads to the formation of pattern with large concentration of small particles under the crest of ripples (Fig.7b). In this region (indicated by an arrow in Fig.7c), the concentration of large particles decreases. This pattern may be compared with pattern shown in Fig. 2cd. Red sand particles during the process of segregation tend to be concentrated under the crests.

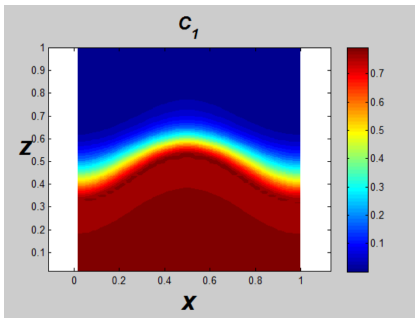

a) Final distribution of large particles

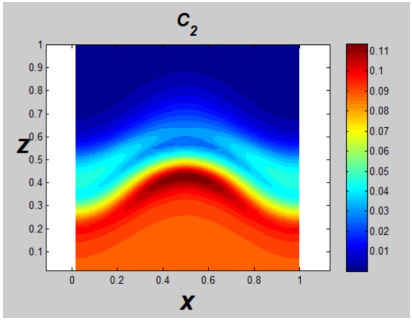

b) Final distribution of small particles

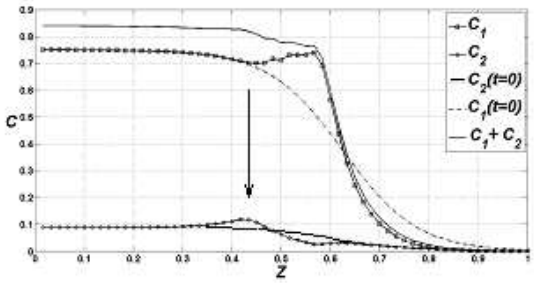

c) Dependence of particle concentrations on vertical coordinate z under the crest of sand ripples x=0.5

Fig.7

Conclusions

Using nonlinear diffusion equation, we have found two dimensional segregation patterns for mixtures of particles with different diameters and different densities. Patterns observed in numerical simulations are similar to patterns investigated in physical experiments. At least it is possible to find the same topological features in experimentally and numerically obtained patterns. The main problem is connected with the choosing of coefficients in differential equations. By now there is no any regular method to determine these coefficients.

References

1. T.D.Chu. Dynamique sédimentaire en zone côtière dans le cas de sédiments multi-classes. Thèse Le Havre 2012.
2. H.C.M. Fernandez, J.J.Arenson, Y.Levin and M.Sellitto. A nonlinear diffusion model for granular segregation. *Physica A* vol. 327, 94-98, 2003.
3. J.J.Arenson, Y.Levin and M.Sellitto Slow dynamics under gravity: a nonlinear diffusion model. *Physica A* 325, 371-395, 2003.
4. .E.Guyon, J.-P. Hulin, L.Petit. Hydrodynamique physique. CNRS Edition Paris, 2001, 676 p.